Amorphous carbon nanotubes based composite for efficient ORR

A thesis submitted towards partial fulfilment of the requirements for the degree of

Master of Technology in

Nanoscience and Technology

Submitted by

SOURAV CHOWDHURY

EXAM ROLL NO: M4NST19003

REG NO: 141065 OF 2017-2018

Under the guidance of

Prof. Kalyan Kumar Chattopadhyay

School of Materials Science and Nanotechnology

Jadavpur University

Kolkata -700032

Course affiliated to

Faculty of Engineering and Technology

Jadavpur University

Kolkata-700032

India

2019

M.Tech. (Nanoscience and Technology) course affiliated to
Faculty of Engineering and Technology
Jadavpur University
Kolkata, India

CERTIFICATE OF RECOMMENDATION

This is to certify that the thesis entitled **"**Amorphous carbon nanotubes based composite for efficient ORR **"** is a bonafide work carried out by **SOURAV CHOWDHURY** under our supervision and guidance for partial fulfilment of the requirement of Master of Technology in Nanoscience and Technology in School of Materials Science and Nanotechnology during the academic session 2017-2019.

THESIS ADVISOR
Prof. Kalyan Kumar Chattopadhyay
School of Materials Science and Nanotechnology,
Jadavpur university,
Kolkata-700 032

DIRECTOR
Dr. Chandan Kumar Ghosh
School of Materials Science and Nanotechnology,
Jadavpur University,
Kolkata-700 032

DEAN
Faculty Council of Interdisciplinary Studies, Law and Management
Jadavpur University,
Kolkata-700 032

M.Tech. (Nanoscience and Technology) course affiliated to
Faculty of Engineering and Technology
Jadavpur University
Kolkata, India

CERTIFICATE OF APPROVAL **

This foregoing thesis is hereby approved as a credible study of an engineering subject carried out and presented in a manner satisfactorily to warranty its acceptance as a prerequisite to the degree for which it has been submitted. It is understood that by this approval the undersigned do not endorse or approve any statement made or opinion expressed or conclusion drawn therein but approve the thesis only for purpose for which it has been submitted.

Committee of final examination for evaluation of Thesis

** Only in case the thesis is approved.

DECLARATION OF ORIGINALITY AND COMPLIANCE OF ACADEMIC ETHICS

I hereby declare that this thesis contains literature survey and original research work by the undersigned candidate, as part of his **Master of Technology** (Nanoscience and Technology) studies during academic session 2017-2019.

All information in this document has been obtained and presented in accordance with academic rules and ethical conduct.

I also declare that, as required by this rules and conduct, I have fully cited and referred all material and results that are not original to this work.

NAME: SOURAV CHOWDHURY

ROLL NUMBER: M4NST19003

THESIS TITLE: Amorphous carbon nanotubes based composite for efficient ORR

SIGNATURE: DATE:

DECLARATION OF ORIGINALITY AND COMPLIANCE OF ACADEMIC ETHICS

I hereby declare that this thesis contains literature survey and original research work by the undersigned candidate, as part of his **Master of Technology (**Nano Science and Technology) studies during academic session 2017-2019.

All information in this document has been obtained and presented in accordance with academic rules and ethical conduct.

I also declare that, as required by this rules and conduct, I have fully cited and referred all material and results that are not original to this work.

NAME: SOURAV CHOWDHURY

ROLL NUMBER: M4NST19003

THESIS TITLE: Amorphous carbon nanotubes based composite for efficient ORR

SIGNATURE: **DATE:**

Dedicated to my

PARENTS

for their support and encouragement.....

ACKNOWLEDGEMENT

This work described in the thesis titled "Amorphous carbon nanotubes based composites for efficient ORR and resistive switching applications" was initiated in the Thin Film & Nanoscience Laboratory, Jadavpur University in the year 2018 and would not have been possible without the immense support and invaluable advice from the members of this lab who are nothing less than a large well bonded family.

I could never have reached the heights or explored the depths without the support, guidance and efforts of a lot of people. Prior to everything, I would like to express my earnest gratitude to my project supervisor **Prof. Kalyan Kumar Chattopadhyay** for granting me this opportunity to work under his esteemed guidance in a laboratory that is well equipped with all necessary advanced equipment. His enthusiasm, unlimited support and profound knowledge have been a major learning experience throughout my research work at the Jadavpur University.

I wish to express my sincere thanks to Dr. Chandan Kumar Ghosh, Dr. Mahua Ghosh Chowdhury, Prof. G. C. Das, Dr. Sourav Sarkar and Honourable Dean, Faculty of Interdisciplinary Studies, Law & Management for their encouragement during the course.

I would like to express my heartiest thanks to Mr. Biswajit Das for his ideas throughout my project and to make my project successful. Without his guidance, support and immense enthusiasm it would have been impossible for me to complete this project.

I am also thankful to Anjan da, Saikat da, Dimitra di, Antika di, Rimpa di, Madhupriya di, Nripen da, Bikram da,Tufan da, Subhankar da, Koushik da, Souvik da and all others for their helpful and supportive nature. My heartiest gratitude to my parents, friends and outstanding labmates Debnath, Pratik, Sumit, Ankit, Pulok da, Utpal,Ankita for their valuable discussions and constant cooperation throughout the project work.

Date: [Sourav Chowdhury]

ABSTRACT:

The electrochemical energy storage and conversion has become one of the most imperative ways in solving tribulations arisen from the global energy demand and environmental brunt of traditional fossil fuel. As vital process in practical operation of fuel cells and metal-air, electrochemical oxygen reduction reaction (ORR) has received extensive attention. ORR is the key limiting in the energy conversion efficiency of fuel cells, and also critical for better understanding of the reaction mechanism of oxygen electrode in metal-air batteries. The sluggish kinetics of ORR makes catalysts highly demanding.ORR can undergo two electron transfer path producing H_2O_2 as the intermediate or four electron transfer path producing H_2O as the final product. The latter is more favorable as the reduction rate is much faster and could give higher energy conversion efficiency. Traditionally, platinum (Pt) based novel metal catalysts that possess high activity and favorable stability was viewed as the best ORR catalyst, receiving tremendous scientific interests during the early years. However, it is well known that Pt-based catalysts suffer from drawbacks like scarcity, high cost, poor durability and easily inactivated by CO poisoning. Hence, a lot of efforts have been devoted into designing of metal free ORR catalysts as the alternatives of traditional PT-based catalysts. So, here we used a novel amorphous carbon nanotube – reduced graphene oxide (aCNT-rGO) nano composite as ORR catalyst which shows four electron transfer path producing H_2O as final product which is desirable. This robust and low cost composite may be a competitive candidate for the ORR catalyst.

TABLE OF CONTENTS

Chapter 1

1. Introduction

1.1 Introduction to Nanoscience &Nanotechnology :

Nanotechnology is science, engineering, and technology conducted at the nanoscale, which is about 1 to 100 nanometers. One nanometer is a billionth of a meter, or 10^{-9} of a meter. Nanotechnology is manipulation of matter on an atomic, molecular, and supra molecular scale. Nanotechnology as defined by size is naturally very broad, including fields of science as diverse as surface science, organic chemistry, molecular biology, semiconductor physics, energy storage, micro fabrication, molecular engineering, etc. The associated research and applications are equally diverse, ranging from extensions of conventional device physics to completely new approaches based upon molecular self-assembly, from developing new materials with dimensions on the nanoscale to direct control of matter on the atomic scale.

1.1.1 What is nanotechnology?

Most definitions revolve around the study and control of phenomena and materials at length scales below 100 nm and quite often they make a comparison with a human hair, which is about 80,000 nm wide.

It seems that a size limitation to the 1-100 nm range, the area where size-dependant quantum effects come to bear, would exclude numerous materials and devices, especially in the pharmaceutical area, and some experts caution against a rigid definition based on a sub-100 nm size. This definition reflects the fact that quantum mechanical effects are important at this quantum-realm, and so the definition shifted from a particular technological goal to a research category inclusive of all types of research and technologies that deal with the special properties of matter which occur below the given size threshold. It is therefore common to

see the plural form "nanotechnologies" as well as "nanoscale technologies" to refer to the broad range of research and applications whose common trait is size.

Another important criteria for the definition is the requirement that the nano-structure is man-made, i.e. a synthetically produced nanoparticle or nanomaterial. Otherwise we would have to include every naturally formed biomolecule and material particle, in effect redefining much of chemistry and molecular biology as 'nanotechnology‘.

1.1.2 How it started?

The ideas and concepts behind nanoscience and nanotechnology started with a talk entitled ―There‘s Plenty of Room at the Bottom‖ by physicist Richard Feynman at an American Physical Society meeting at the California Institute of Technology on December 29, 1959; long before the term nanotechnology was used. In his talk, Feynman described a process in which scientists would be able to manipulate and control individual atoms and molecules. Thus, physicist Richard Feynman is called the father of nanotechnology.

1.1.3 Who coined the term Nanotechnology?

The term was coined in 1974 by Norio Taniguchi of Tokyo Science University to describe semiconductor processes such as thin-film deposition that deal with control on the order of nanometers. It wasn't until 1981, with the development of the scanning tunneling microscope that could "see" individual atoms, with which modern nanotechnology began.

Inspired by Feynman's concepts, K. Eric Drexler used the term "nanotechnology" in his 1986 book *Engines of Creation: The Coming Era of Nanotechnology*, which proposed the idea of a nanoscale "assembler" which would be able to build a copy of itself and of other items of arbitrary complexity with atomic control.

Today, scientists and engineers are finding a wide variety of ways to deliberately make materials at the nanoscale to take advantage of their enhanced properties such as higher

strength, lighter weight, increased control of light spectrum, and greater chemical reactivity than their larger-scale or bulk counterparts.

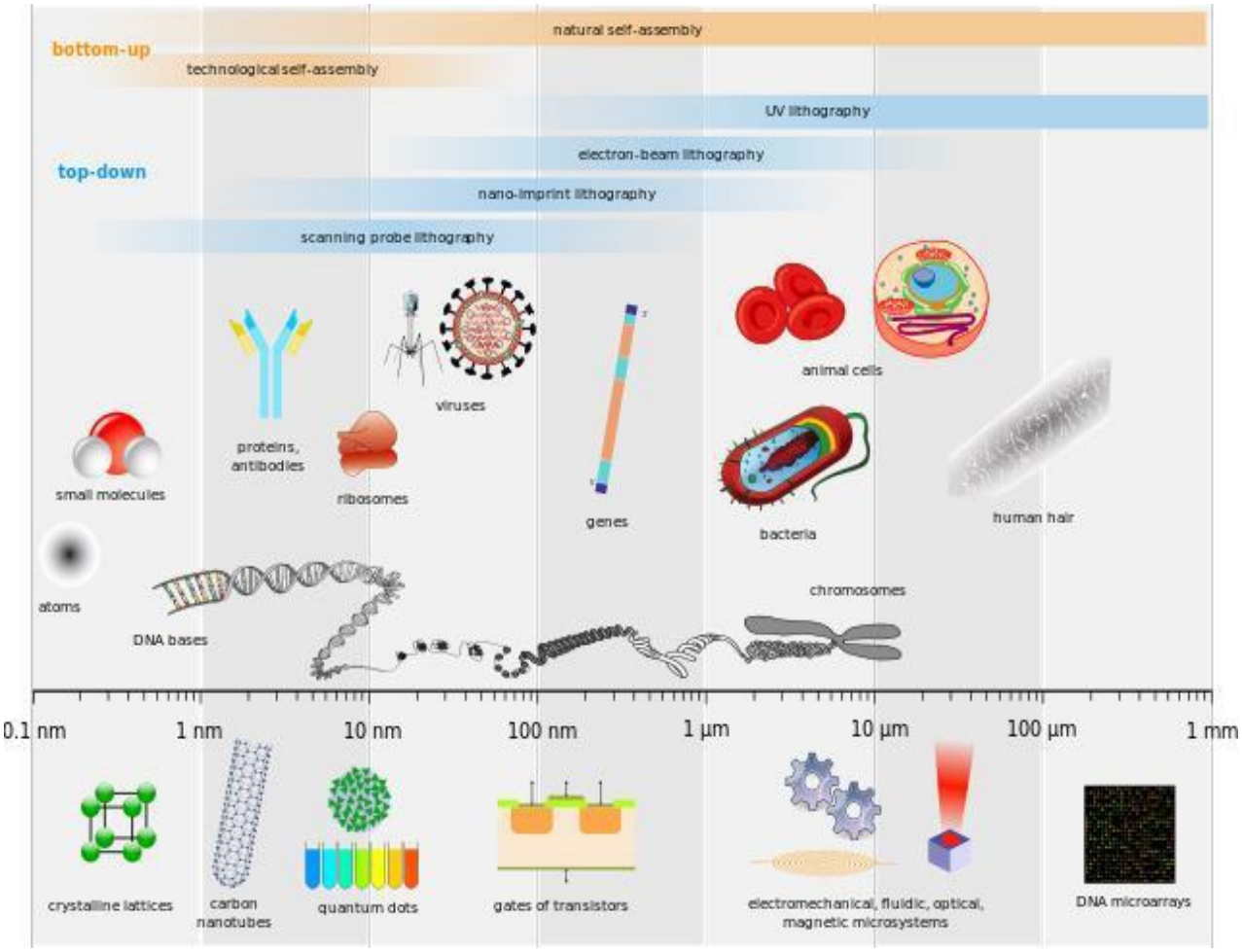

Fig.1.1: Schematic diagram of nanotechnology and its size comparison

1.1.4 A brief history of nanotechnology:

- **1959:** Physicist Richard Feynman gave a radical lecture at an American Physical Society meeting at Caltech titled ―‖There‗s plenty of room at the bottom‖.
- **1974:** Nanotechnology- Professor Norio Taniguchi for the first time uses the termnanotechnology [4].
- **1981:** IBM develops Scanning Tunnelling Microscope [5].
- **1985:** Buckyball- Scientists at Rice University and University of Sussex discoverFullerene (C_{60}) [6].
- **1986:** ‗Engines of Creation‗- First book on nanotechnology by K. Eric Drexler [7].Atomic Force Microscope invented by Binnig, Quate, and Gerbe.
- **1989:** IBM logo made with individual atoms.
- **1991:** Carbon Nanotubes discovered by S. Ijima.
- **1999:** Nano medicine- First Nano medicine book by R. Freitas.

1.1.5 What distinguishes nanomaterial from bulk?

While most micro structured materials have similar properties to the corresponding bulk materials, the properties of materials with nanometre dimensions are significantly different from those of atoms and bulk materials. Among the characteristics of nanomaterial that distinguish them from bulk materials, it is important to note the following:

- Large fraction of surface atoms;
- High surface energy;
- Spatial confinement
- Reduced numbers of imperfections that do not exist in the corresponding bulk materials [1].

The use of nanomaterial provides the following advantages [1].

First, all nanomaterial consist of very small particles. This is the first advantage of nanomaterial and nanotechnologies, promoting attainment of super miniaturization. Because they are small, nanostructures can be packed very closely together. As a result, on a given unit of area one can locate more functional nanodevices, which is very important for Nanoelectronics. Their high packing density has the potential to bring higher area and volume capacity to information storage and higher speed to information processing (because electrons require much less time to move between components). Thus, new electronic device concepts, smaller and faster circuits, more sophisticated functions, and greatly reduced power consumption can all be achieved simultaneously by controlling nanostructure interactions and complexity.

Second, because of their small dimensions, nanomaterials have large specific surface areas, accelerating interactions between them and the environment in which they are located. Nanoparticles have a much larger surface area per unit of mass compared with larger particles. Because growth and catalytic chemical reactions occur at surfaces, this means that materials in nanoparticle form will be much more reactive than the same mass of material made up of larger particles. A strong increase in the participation of surface atoms in the physical and chemical properties of nanomaterials is another consequence of a decrease in particle size.

It is known that the volume of an object decreases as the third power of its linear dimensions, but the surface area decreases only as its second power. In case of nanoparticles, the surface area-to-volume ratio (the ratio between surface and bulk atoms) increases than that of bulk.

The variation of surface or volume ratio as a function of particle size is given in Fig.1.3.

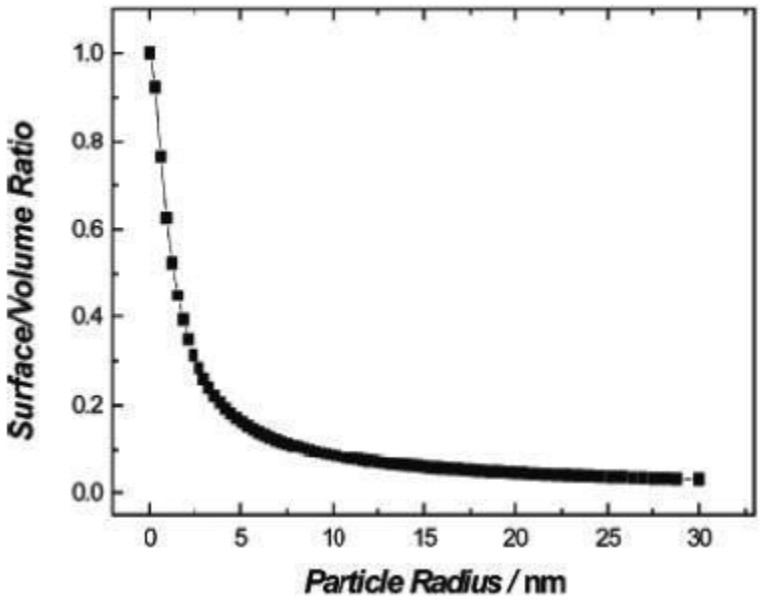

Fig.1.2: Surface/volume ratio as a function of particle size

It is known that atoms on the surface of nanoparticles have unusual properties. These surface atoms make nanoparticles very different from just small particles, because not all bonds of surface atoms with neighbouring atoms are enabled. For atoms on uneven surfaces, no saturation of the bonds is even higher. For this reason, corner atoms normally have the highest affinity to form bonds to adsorbate molecules, followed by edge and in-plane surface atoms, a fact that is of great importance for catalytic activity. Alternatively, because of their low stabilization due to low coordination, edge and in particular corner atoms are often missing on single crystals, even in thermodynamic equilibrium [9]. Recently, size-dependent variation in oxidation state and lattice parameter has been reported for cerium oxide nanoparticles [10].

As a result of the changes that occur in particles with a decrease of particle size, nanomaterials can have extremely high biological and chemical reactivity. For example, catalytically active nanomaterials allow accelerating either chemical or biochemical reactions by tens of thousands, and even a million times. This attribute explains even 1 g of nanomaterial can be more effective than 1 ton of a similar but macro substance.

Another aspect we must consider is that the free surface is a place of accumulation (sink) of crystallographic defects. At small particles sizes, the surface concentration of such defects increases considerably. Hardeveld and Hartog in 1969 calculated classically and showed that the largest changes of proportions between facets, edges, corners, and micro defects at the surface occur between 1 and 5 nm [11]. As a result, strong lattice distortion and even a change of lattice type can take place on the surface layer. In fact, due to accumulation of structural defects and chemical impurities on the surface, we can observe purification of the bulk area of the nanoparticles.

An important specific characteristic of nanomaterial properties (we mean here polycrystalline materials with grain size less than 40 nm) is an increase of the role of interfaces with decrease of the size of grains or crystallites in nanomaterials. Experimental research has shown that the state of grain boundaries has a non-equilibrium character, conditioned by the presence of the high concentration of grain boundary defects. This non-equilibrium is characterized by extra energy of the grain boundaries and by the presence of long-range elastic stress. At the same time, the grains have ordered crystallographic structure, while the grain boundary defects act as a source of elastic strains. Non-equilibrium of the grain boundaries initiates the occurrence of the lattice distortion, the change of interatomic distances, and the appearance of sufficient displacement of atoms, right up to loss of an ordered state.

Another important factor peculiar to nanoparticles is their tendency to aggregation. The possibility of migration (diffusion) of either atoms or groups of atoms along the surface and the boundaries, as well as the presence of attractive forces between them, often leads to processes of self-organization into various cluster structures. This effect has already been used for creation of ordered nanostructures in optics and electronics.

One more important aspect of nanomaterial properties is connected with the fact that, during transport processes (diffusion, electro- and thermal conductivity, etc.), there are certain effective lengths of free path of a carrier of this transport (L_e), such as phonon and electron mean free paths, the Debye length, and the exciton diffusion length for certain polymers.

While proceeding to sizes smaller than L_e , transport speed starts to depend on both the size and the shape of the nanomaterial; generally, the transport speed increases sharply [12].

The principal characteristics of nanomaterials are conditioned by not only by their small the size, but also by the appearance of new quantum mechanical effects in a dominating role at the interface (Esaki 1991 [13]; Serena and Garcia 1997 [14]). Those quantum size effects occur at a critical size, which is proportionate with the so-called correlative radius of one or another physical phenomena, for example, with the length of the free path of electrons or photons, the length of coherence in a superconductor, sizes of magnetic domains, and so on. As a rule, quantum size effects appear in materials with crystallite sizes in the nano range D <10 nm. As a result, in nanomaterials with characteristic size, one can expect the appearance of effects which cannot be observed in bulk materials.

1.1.6: Classification of Nanomaterials

Classification	*Examples*
Zero dimension< 100nm	Particles, quantum dots, hollow Spheres, etc.
One dimension < 100nm	Nanorods, nanowires etc.
Two dimensions < 100nm	Tubes, fibres, platelets, etc.

On the basis of phase composition, nanomaterials in different phases can be classified as,

- Single phase solids include crystalline, amorphous particles and layers, etc.
- Multi-phase solids include matrix composites, coated particles, etc.
- Multi-phase systems include colloids, aero gels, Ferro fluids, etc.

1.1.7 Synthesis of Nanomaterials:

In order to explore the unique physical properties & phenomena and also to realize the useful applications of nanostructures and nanomaterial, the ability to fabricate and process nanomaterial and nanostructures is the first hurdle in nanotechnology. The following schematic diagram in Fig. 1.4 shows the two significant approaches in the synthesis of nanomaterial.

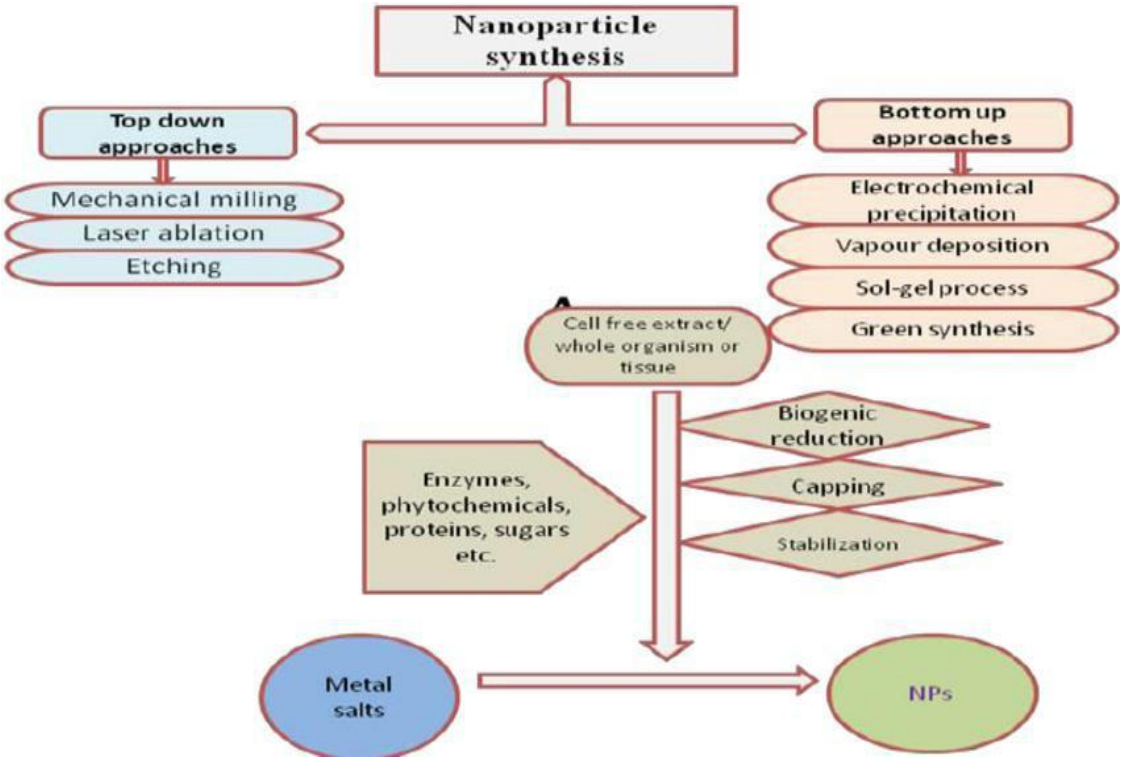

Fig.1.4: Schematic diagram of different synthesis approaches of nanomaterials

For the fabrication and processing of nanomaterial and nanostructures, the following challenges must be taken care of [1]:

- Overcome the huge surface energy, a result of enormous surface area or large surface-to- volume ratio.

- Ensure all nanomaterial with desired size, uniform size distribution, morphology, crystallinity, chemical composition, and microstructure which result in desiredphysical properties.

- Prevent nanomaterial and nanostructures from coarsening through either Ostwald ripening or agglomeration.

(1) According to growth media:

a. Vapour phase growth, including laser reaction pyrolysis for nanoparticle synthesis andatomic layer deposition (ALD) for thin film deposition.

b. Liquid phase growth, including colloidal processing for the formation of nanoparticles andself-assembly of monolayers.

c. Solid phase formation, including phase segregation to make metallic particles in glass

matrix.

(2) According to the form of products:

a. Nanoparticles by means of colloidal processing, flame combustion and phase segregation.
b. Nano rods or nanowires by template-based electroplating, solution liquid- solid growth(SLS), and spontaneous anisotropic growth.

c. Thin films by molecular beam epitaxy (MBE) and atomic layer deposition (ALD).

(3) 'Top Down' and 'Bottom Up Approach':

The top down approach uses traditional methods to guide the synthesis of Nano scale materials [1, 15]. The paradigm proper of its definition generally dictates that in the top down approach it all begins from a bulk piece of material, which is then gradually or step by step removed to form objects in the nanometre-size regime. Well known techniques such as photo lithography and electron beam lithography, anodization, ion and plasma etching all belong to this type of approach. The bottom up approach is exactly the opposite of top down approach.

In this case instead of starting with large materials and chipping it away to reveal small bits of it, it all begins from atoms and molecules that get rearranged and assembled to large nanostructures. It is the new paradigm for synthesis in the nanotechnology world as the bottom up approach allows a creation of diverse types of nanomaterial, and it is likely to

revolutionize the way of material fabrication. Schematic representation of Bottom up and Top down approach is shown in Fig.1.5.

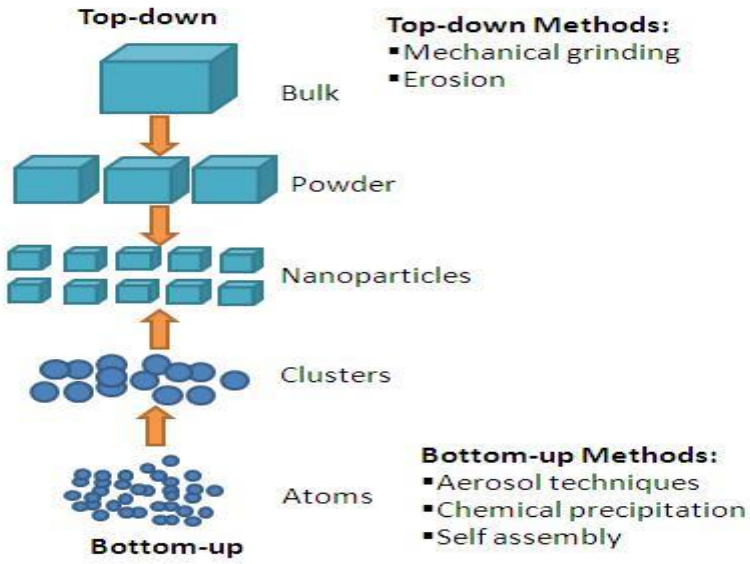

Fig.1.5: Schematic diagram of Top Down and Bottom Up Approach [7]

Attrition or Milling is a typical top down method in making nano particles, whereas the colloidal dispersion is a good example of bottom up approach in the synthesis of nano particles.

(4) Self-assembly:

One bottom-up method is nature's way; ***—self-assembly”***. Self-organizing processes are common throughout nature and involve components from the molecular (e.g. protein folding) to the planetary scale (e.g. weather systems) and even beyond (e.g. galaxies).

1.1.8 Applications of Nanotechnology

Nano technological application is extended in different field of research with various unique applications. When a particle is shrunk to nano-scale, several properties of the material change in accordance with size. So it gives new applications in several fields. As due to the size the surface to volume ratio increases, it gives more surface area to react. Several optical as well as mechanical properties are also dependent on the diameter or the size of particles. The following diagram of **Fig.1.6** shows some few such applications.

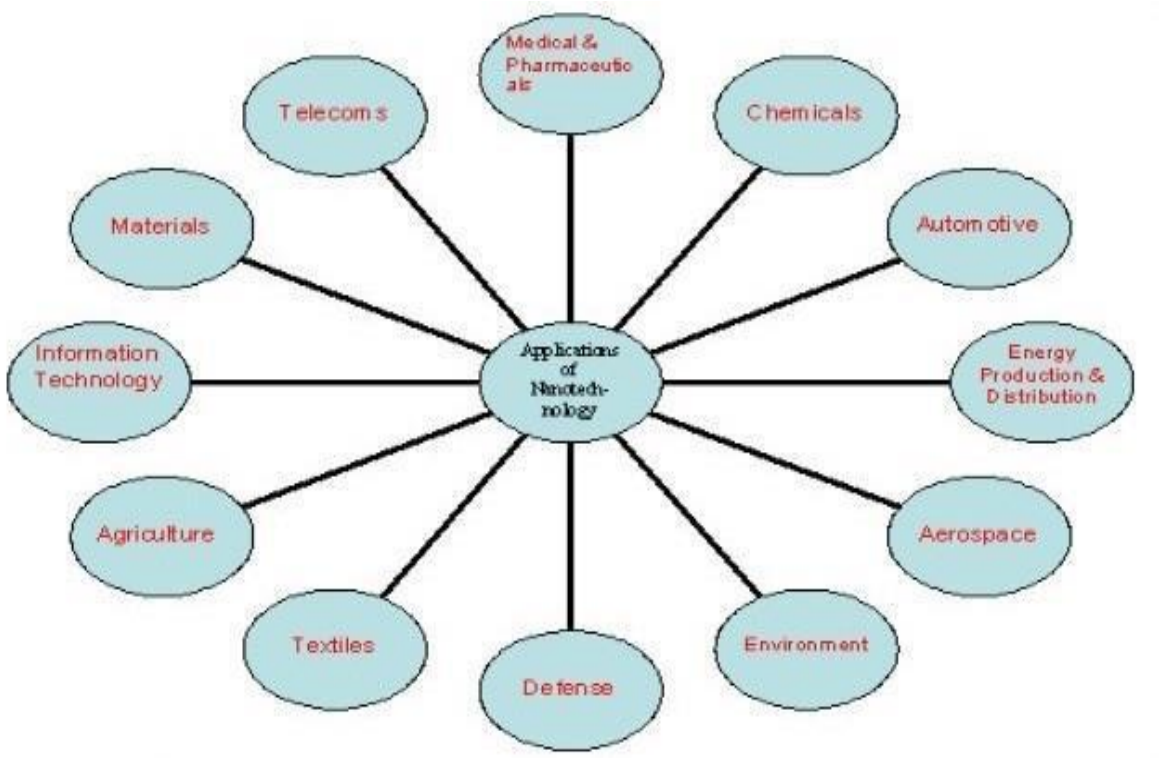

Fig.1.6: Applications of Nanotechnology

Nanotechnology has innumerable applications in variety of diverse fields all of which are interconnected with each other. The modern world has burgeoned in a consequential extent with the advent of newer technologies based on Nano science [17]. The applications include nanoscale pattering of electronic circuits, high density data storage, quantum computers, fuel cell catalysts, environmental catalysts, industrial catalysts, waste water treatment, functional nanocomposites, food packaging, food processing catalysts, hydrogen production photocatalysts, automotive catalysts, fuel additive catalysts, lithium ion battery electrodes, natural or synthetic polymer hybrid fibres, reinforced plastics, controlled drug release, cancer therapy, drug delivery, bio imaging, bio markers, hyperthermic treatment, MRI contrast agents, IR contrast agents, ultra violet protection like sunscreens, antioxidants, ultra violet blocking coatings, water resistant coatings, gas barrier coatings, anti-microbial coatings, self-cleaning building surface, food quality and safety analysis sensors, chemical sensors, gas sensors, high sensitive sensors, pollution monitoring sensors, functional nanocomposites, nano pigments, super thermal-conductive liquid, nano phosphors for display, super plastic ceramics, transparent conductive polymer films, chemical mechanical planarization, nano inks, single electron transistors, quantum lasers, high power magnets, pollutant scavengers, interactive food, neutraceutical, fungicides and pesticides, medical textiles, technical textiles, heat retaining textiles, self-cleaning textiles, anti-stain textiles, electro-conducting textiles, ultra violet blocking textiles, wound dressing, dental ceramics, bone growth, tissue cells engineering, molecular tagging, dye sensitized solar cells, paint-on solar cells, hydrogen storage materials, bio-composites, Ferro-fluids, refractive index engineering, aerospace engineering and many others. Detail applications in some important fields are given below:

➢ Nanotechnology in Energy and Environment:

Energy crisis and environmental pollution in present days have severe negative impact in human life. To provide sufficient energy to the developing world, nanotechnology is the key factor because less expensive improved energy can be produced through suitable nanomaterial. Recent nanotechnology projects to diminish the energy crisis is related to the parameters like storage, conversion, sufficient super capacitance and recyclability production with the help of small amount of nanomaterial, thermal insulation increment etc. Energy application with the help of nanomaterial:

(1) Fuel cell (e.g. CNT) for hydrogen storage and related automobile applications.

(2) Cheap, light weight and more efficient metal oxide nanomaterial photovoltaic application for the purpose of water splitting and efficient dye sensitized solar cell.

(3) Nanotechnology can be used to the further reduction of combustion engine pollutants by nanoporous filters; this can clean the exhaust mechanically.

(4) Nanotechnology in water disinfection with the help of nanostructured photosensitized catalyst and further step towards environmental safe and green technologies.

(5) Solid state lightening is a powerful tool to reduce total electricity consumption by 10% and cut carbon emission by the equivalent of 28 million tons/year.

➢ Nanotechnology in Flexible Electronics:

Nanotechnology in electronic industry is gradually becoming popular because smaller size and compact design of electronic devices can ensure faster processing, reduction of delay in circuitry and processing power consumption. Nanotechnology in electronics industry introduces microprocessors less than 100 nanometres (nm) in size. However, Nanoelectronics

is basically the extension of microelectronics and research in Nano electronics will develop CNT, Graphene based flexible independent electronic devices in future.

(1) CNT based field emission display is highly efficient because light weight CNT can be used as field emitters with extremely high efficiency for field emission displays (FED) with very low power consumption.

(2) Nanotechnology is employed to increase the density of memory chips. Researchers are developing a type of memory chip with a projected density of one terabyte of memory per square inch or greater. Integrated nanosensors are used for collecting, processing and communicating massive amounts of data with minimal size, weight, and power consumption.

(3) Research in nanotechnology introduces transistors with Graphene and CNT as active materials and CNT transistor based processor for computer application is about to commercialize in future market. Due to their smaller size and lower power consumption CNT and Graphene based transistors are easy to integrate in the integrated circuits.

(4) Large magnetic moment and adequate coercivity nanomaterial can help to produce magneto caloric effect on a particular scale so that refrigeration could be possible without need of refrigeration fluids.

➢ Nanotechnology in Health and Medicine:

Nanotechnology has a high impact on the research and applications related to biology and medicine. Nano-drug delivery is the safest procedure for medication because small quantity of nanomaterial can help to recover with reducing side effects. Nano medicine has also the potential to enable early detection and prevention, and to essentially improve diagnosis, treatment and follow-up of diseases with the help of bio-sensors.

(1) Carbon nanotubes have promising application for the development of advanced biosensors with novel features.

(2) CNT, though inert, can be functionalized at the tip with a probe molecule. Their study uses AFM as an experimental platform. i. Leukaemia cells identification

ii. Catheter development.

(3) Nano devices can make gene sequencing more efficient.

(4) Tissue engineering makes use of artificially stimulated cell which can help in transplantation of organs or artificial implants.

(5) The technology is also being used to develop sensors for cancer diagnostics.

➢ Nanotechnology in Transportation:

Nanomaterial is used as faster and cost effective new fuel source. The main advantage of using nanomaterial is light weight so that easy to carry in fuel chamber of cars and aeroplanes.

(1) Suitable Nanomaterials can effectively reduce the emission of pollutants in the process of incomplete combustion in engine. Nano Twin Technologies has recently released an air filter to remove hazardous chemicals from the air in car cabins.

(2) Nanoparticles of inorganic clays and polymers are an effective alternative for carbon black tires results in environmental friendly, wear resistant tires. Frictional resistant tires are also made possible through Nano science.

(3) Nano coating of metallic surfaces such as steel to achieve super-hardening, low friction, and enhanced corrosion protection.

➢ Nanotechnology in Defence and Security:

Nanotechnology will lead to higher protection, more lethality, longer endurance and better self-supporting capacities of future combat soldiers. Substantial advantages are expected to be gained which include threat detection, novel electronic display and interface systems, as

well as a pivotal role for the development of miniaturised unmanned combat vehicles and robotics. Nanotechnology will also enable small portable sensor systems capable of identifying chemical, biological and nuclear, radiation, or explosive threats.

➢ Nanotechnology in Information & Communication:

Electronic memory designs in the past have largely relied on the formation of transistors. The miniaturization of electronic industry has been the driving force behind the rapid research and development of Nano science and technology. Continuing to shrink silicon chips is getting expensive and difficult. Chips built using the molecular transistors are the industry's best hope for building faster, cheaper computers well into this century. "With the electronics we're talking about, we're going to make a computer that doesn't just fit in your wristwatch, not just in a button on your shirt, but in one of the fibres of your shirt," says Philip Kuekes, a computer architect at Hewlett-Packard Laboratories. According to the manufacturers, NRAM (Nanotube-based/Non-volatile random access memory) is a universal memory chip suitable for countless existing and new applications in the field of electronics. In the modern communication technology traditional analog electrical devices are increasingly replaced by optical or optoelectronic devices due to their enormous bandwidth and capacity. Two promising examples are photonic crystals and quantum dots. Quantum dots are nanoscale objects, which can be used for the construction of lasers. The advantage of a quantum dot laser over the traditional semiconductor laser is that their emitted wavelength depends on the diameter of the dot. Quantum dot lasers are cheaper and offer a higher beam quality than conventional laser diode.

1.4 References :

1. Nanostructures and Nanomaterials: Synthesis, Properties and Applications; Guozhong Cao.

2. Introduction to Nanoscience, Kai Nordlund; 2005.

3. Iijima, S., 1991; Helical microtubules of graphitic carbon. N*ature*, *354*(6348), pp.56- 58.

4. N. Taniguchi, "On the Basic Concept of 'Nano-Technology'," Proc. Intl. Conf. Prod. Eng. Tokyo, Part II, Japan Society of Precision Engineering, 1974.

5. G. Binnig et al., Phys. Rev. Lett. 49, 57,(1982).

6. Smalley, R.E., 1997. Discovering the fullerenes. *Reviews of Modern Physics*, *69*(3), p.7

7. K.E. Drexler, Engines of creation: The coming era of nanotechnology, (Oxford University Press, Oxford, 1986); K.E. Drexler, C. Terson, G. Pergamit, Unbounding the Future: The Nanotechnology Revolution (Morrow, New York, 1991); K.E. Drexler, Nanosystems: Molecular Machinery, Manufacturing, and Computation,(Wiley, New York, 1992).

8. Burda, C., Chen, X., Narayanan, R. and El-Sayed, M.A., 2005. Chemistry and properties of nanocrystals of different shapes. *Chemical reviews*, *105*(4), pp.1025-1102.

9. Roduner, E., 2006. Size matters: why nanomaterials are different. *Chemical SocietyReviews*, *35*(7), pp.583-592.

10. Deshpande, S., Patil, S., Kuchibhatla, S.V. and Seal, S., 2005. Size dependency variation in lattice parameter and valency states in nanocrystalline cerium oxide. *Applied PhysicsLetters*, *87*(13), pp.133113-133113.

11. Van Hardeveld, R. and Hartog, F., 1969. The statistics of surface atoms and surface sites on metal crystals. *Surface Science*, *15*(2), pp.189-230.

12. Law, M., Goldberger, J. and Yang, P., 2004. Semiconductor nanowires and nanotubes.

13. Tsu, R. and Esaki, L., 1991. Stark quantization in superlattices. *Physical Review B*, *43*(6), p.5204.

14. Costa-Krämer, J.L., García, N., García-Mochales, P., Serena, P.A., Marqués, M.I. and Correia, A., 1997. Conductance quantization in nanowires formed between micro and macroscopic metallic electrodes. *Physical Review B*, *55*(8), p.5416.

15. C.N. chinthamani nagesa ramachandra rao, P.john Thomas, G.U. kulkarni, Nano crystal: synthesis, properties and applications, (2007).

16. Shimizu, T. ed., 2008. *Self-assembled nanomaterials II: Nanotubes* (Vol. 220). Springer.

17. http://www.nanowerk.com/nanotechnology-applications.php

18. Montigaud, H., Tanguy, B., Demazeau, G., Alves, I. and Courjault, S., 2000. C3N4: Dream or reality? Solvothermal synthesis as macroscopic samples of the C3N4 graphitic form. Journal of materials science, 35(10), pp.2547-2552.

19. Y. Gu, L. Chen, L. Shi, J. Ma, Z. Yang and Y. Qian, Carbon, 2003, 41, 2674.

20. Q. Guo, Y. Xie, X. Wang, S. Zhang, T. Hou and S. Lv, Chem. Commun., 2004, 26

21. Z. Yang, Z. Yao, G. Li, G. Fang, H. Nie, Z. Liu, X. Zhou, X. Chen and S. Huang, *ACS Nano*, 2012, **6**, 205-211.

22. S. Zhao, J. Liu, C. Li, W. Ji, M. Yang, H. Huang, Y. Liu and Z. Kang, *ACS Appl. Mater. Inter.*, 2014, **6**, 22297-22304.

23. K. Zhou, W. Zhou, X. Liu, Y. Wang, J. Wan and S. Chen, *ACS Appl. Mater. Inter.*, 2014, **6**,
14911-14918.

24. X. Wang, J. Wang, D. Wang, S. Dou, Z. Ma, J. Wu, L. Tao, A. Shen, C. Ouyang, Q. Liu and S. Wang, *Chem. Commun.*, 2014, **50**, 4839-4842.

25. Z. L. Ma, S. Dou, A. L. Shen, L. Tao, L. M. Dai and S. Y. Wang, *Angew. Chem. Int. Ed.*, 2015, **54**, 1888-1892.

26. S. Chen, J. Y. Bi, Y. Zhao, L. J. Yang, C. Zhang, Y. W. Ma, Q. Wu, X. Z. Wang and Z. Hu,
Adv. Mater., 2012, **24**, 5593-5597.

27. H. L. Jiang, Y. H. Zhu, Q. Feng, Y. H. Su, X. L. Yang and C. Z. Li, *Chem. Eur. J.*, 2014, **20**, 3106-3112.

28. G. Girishkumar, B. McCloskey, A. C. Luntz, S. Swanson and W. Wilcke, *J. Phys. Chem. Lett.*, 2010, **1**, 2193-2203.

29. Y. Shao, S. Park, J. Xiao, J. Zhang, Y. Wang and J. Liu, *ACS Catal.*, 2012, **2**, 844-857.

30. M. M. Montemore, M. A. van Spronsen, R. J. Madix and C. M. Friend, *Chem. Rev.*, 2018, **118**, 2816-2862.

31. K. M. Ervin, I. Anusiewicz, P. Skurski, J. Simons and W. C. Lineberger, *J. Phys. Chem. A*,
2003, **107**, 8521-8529.

32. B. Ruscic, R. E. Pinzon, M. L. Morton, N. K. Srinivasan, M.-C. Su, J. W. Sutherland and J. V. Michae, *J. Phys. Chem. A*, 2006, **110**, 6592-6601.

33. B. B. Blizanac, P. N. Ross and N. M. Markovic, *Electrochim. Acta.*, 2007, **52**, 2264-2271.

34. K. Kato, T. Uda and K. Terakura, *Phys. Rev. Lett.*, 1998, **80**, 2000-2003.

35. A. Ziletti, A. Carvalho, D. K. Campbell, D. F. Coker and A. H. Castro Neto, *Phys. Rev. Lett.*, 2015, **114**, 046801.

36. J. S. Spendelow and A. Wieckowski, *Phys. Chem. Chem. Phys.*, 2007, **9**, 2654-2675.

37. X. Ge, A. Sumboja, D. Wuu, T. An, B. Li, F. W. T. Goh, T. S. A. Hor, Y. Zong and Z. Liu,
ACS Catal., 2015, **5**, 4643-4667.

38. P. Quaino, N. B. Luque, R. Nazmutdinov, E. Santos and W. Schmickler, *Angew. Chem.*

Chapter 2

2. LITERATURE REVIEW

2.1 Introduction to electrocatalyst

Catalysis is the driving force behind the development of the chemical industry, which can not only make us use natural resources more efficiently, but also reduce the pollution in the processes of the chemical industry. In the last century, catalysis has become the foundation of the large-scale production of the chemical and petroleum industry [1–4]. However, there still exist some problems to be solved [5,6]. With the development of nanotechnology, catalysis has ushered in some new challenges and opportunities. In recent years, certain achievements have been made in the metal nanomaterials as heterogeneous catalysts [7–10]. These catalysts have a very high catalytic activity and selectivity for specific reactions. Nanocatalysts for catalytic chemical reactions mainly include the oxidation reaction [7], the reduction reaction [8], coupling reaction [9,10] and the electrochemical reaction [11–15]. They have attracted more and more workers' attention. The main reason why nanomaterials have attracted so much attention is that they are a bridge between atoms and bulk materials. In addition, they have some special properties, such as the surface and interface effect (unusual properties of extremely small crystals that arise from the damage of a boundary between a material and its surrounding environment), small size effect (novel properties of extremely small crystals that arise from the decrease of the atom's density of amorphous nanoparticles near the surface layer), quantum size effect (unusual properties of extremely small crystals that arise from confinement of electrons to small regions of space in one, two, or three dimensions) and macroscopic quantum tunnel effect (when the total energy is less than the barrier height, extremely small crystals can still pass through the barrier.), as well as, some potential applications, such as catalysis, biology, medicine and so on. This review article reviews noble metal nanomaterials as heterogonous catalysts applied into organic reactions and electro-catalysis in our group recently, which intends to combine nanomaterial preparation and organic chemistry or fuel cell systems to find new catalysts for low-cost, highly-selective chemical synthesis that is clean and energy-efficient. In catalytic organic reactions, the transformation of functional groups based on novel nanomaterials, can not only achieve "atom economy", the chemical processes showed low energy consumption and induced low pollution at the same time. In electro-catalysis, the synthesized nanomaterials can enhance electrocatalytic activity for direct oxidation of methanol and formic acid, as well as, meet the demand for clean and energy efficient fuel cell systems. Therefore, we arrange the content of this review in the following way. Firstly, we introduce several platinum (Pt)-based nanocomplexes' synthesis including FePt@Cu nanowires (NWs), Pt@Fe2O3 NWs and Pt@Ir zigzag bimetallic nanocomplexes. The former two kinds of novel NWs were used as "non-support" heterogeneous catalysts in oxidation, while the latter one exhibited good performance in reduction. Secondly, the facile synthesis of hybrid nanostructures (such as necklace-like Pt-Au nanostructures, three-dimensional Pt/Pd bimetallic nanodendrites and

Au-Pt bimetallic nanocomplexes) is reviewed to demonstrate their high stabilities as electrocatalysts for the oxygen-reduction reaction. Thirdly, we discuss the synthesis of several other noble metal nanomaterials including Au, Pd and Ag, but also their excellent catalytic abilities. Lastly, we attempt to point out a novel solution of "green chemistry" based on heterogeneous nanocatalysts, in order to stimulate the future development of nanomaterials that ultimately contributes to addressing the current challenges and that leads to new opportunities in nanomaterials and nanocatalysis.

2.2 Traditional pt based ORR electro catalyst

It is generally accepted that fuel cells give an ultimate energy solution because of their high efficiency, zero emission, quiet process and unlimited renewable source of reactants.1-Stationary power, transportation and portable power are the three major markets for fuel cell technology. Among various fuel cells, proton exchange membrane (PEM) fuel cell with advantages of low operating temperature, quick starting and compact stack, attracts much attention worldwide. A recent landmark event in the fuel cells is Toyota launching its hydrogen fuel cell vehicle "Mirai" at the Los Angeles Auto Show, November 2014. This is one of the first such mass vehicles sold commercially. This arouses a new fuel cell tide. However, the sluggish rate of oxygen reduction reaction (ORR)at the cathode is still a major challenge in research and development of PEM fuel cells. Platinum (Pt) is the best single metal electrocatalyst for ORR with high activity and durability in acid,6 while its ORR rate is ~5 orders of magnitude slower

than the hydrogen oxidation reaction at the anode. Consequently, the cathode of a PEM fuel cell typically contains80~90 % of the total Pt in the stack. Due to the scarcity and high cost of platinum, the target of Pt loading of a total (anode+ cathode) is required below 0.125 mg cm-2 in 2017 according to US Department of Energy (DOE), comparing with present status of ~0.4 mg cm-2 or more used on cathode.7 Reducing Pt loading of the cathode without loss in the performance is the subject of most of the electrocatalytic studies. Until now, Pt based electrocatalysts are currently the only choice in practical PEM fuel cells. Although many efforts on Pt-free electrocatalysts, like non-precious transition metals, metal nitrides and the nanoscale carbon-based metal-free electrocatalysts, are in the investigation, it is rather difficult to assume that these catalysts will be commercially available for the fuel cell industry due to the poor stability and limited performance of these kinds of catalysts.9,10 Most emerging approaches still focus on controlling the surface structure and surface electronic state (or composition) of platinum nanoparticles(NPs) to achieve higher ORR activity with less Pt. Some new synthetic routes have delivered such "designer nanoparticles" Pt-based electrocatalysts can be class into three main groupings: pure platinum, platinum

alloys and core-shell platinum structure, which show different activity and stability after controlling structure/geometry and electronic state. Alloying Pt with other metals can vary the bond strength between the electrocatalyst and the ORR intermediates, leading to higher ORR catalytic activity. It can also help the cost effectiveness of a fuel cell by reducing the total Pt content in the catalyst. Beside the enormous number of binary alloy catalysts for ORR explored for several decades, the ternary, quaternary and quinary alloys have now been investigated in the past few years.12-16 Stamenkovic *et al*.demonstrated that the Pt3Ni (111) surface possesses 90-foldmore activity than the current commercial Pt/C catalysts for PEM fuel cells. Pt xGd NPs exhibited an outstanding activity of3.6 Amg-1 Pt at 0.9 V RHE in liquid half cells, a little lower thanPt3Ni (111). However, Pt alloys are thermodynamically unstable under fuel cell conditions. The transition metal alloyed with platinum tends to dissolve into the electrolyte via process known as de alloying. The leakage level (or Pt enrichment) and the thickness of the de alloyed region vary with different alloys, preparation techniques and electrochemical treatments. Although some Pt alloy catalysts with advanced nanostructures have shown remarkable activity, the dissolution of metals, including Pt and alloyed base metals, in fuel cell operation environments could cause catalyst degradation and pollute electrolyte membranes. This still remains an issue. Another issue may be the low retention of active catalyst nanostructure during fuel celloperation.16The idea of core−shell structure is to improve the unlizanon of Pt atoms by depositing or forming a thin Pt-based shell(several atom layers) around a less expensive core, such as Pd-,Ru-, and Re-based NPs.5 The Pt “shell” could be in different forms, like Pt-rich surface layer by electrochemical de alloying.

20 or annealing21 or acid leaching14, Pt over layer by seeds-based chemical reduction22, and Pt monolayer by under potential deposition23,24. Chung *et al*.25 demonstrated that the ORR of the NPs is significantly affected by their sub surface composition rather than the bulk composition. An appropriate Pt-skin thickness and modulated subsurface structure induce geometric and electronic effects that enhance the ORRactivity.9 However, the surface segregation, the composition change for Pt alloys and less sufficient Pt surface coverage for Pt monolayer affect the stability and activity of thesecatalysts.9,21With the advances in *in-situ* characterization techniques significant progresses in Pt catalysts with tailoring structure have been made. Electrochemical reactions with tuning selectivity become possible by atomically dispersed platinumcatalyst.30 As Pt-based electro-catalysts, pure platinum, platinum alloys and core-shell structures have their own advantages and disadvantages.

2.2 Limitations Pt based as ORR electro catalyst

Significant progresses have been made recently in the studies of the Pt based ORR catalysts over various carbon supporting materials. The major objectives of these studies are: 1) to design and prepare highly active Pt catalyst with low Pt content and with excellent durability; 2) to get a fully understanding of Pt ORR catalyst. From the results reported, the following conclusions can be made: 1) the size of the Pt NPs has a significant effect. Based on the catalyst components, supporting materials and reaction conditions, an optimal catalyst size exists. However, the size effect is obviously a complicated issue for the supported Pt catalysts because of the complex reaction mechanism of ORR and complicated structural influencing factors. The present studies conducted for the size effects did not maintain the same catalyst structure with the same defect status because of the difficulty in the structure and defect control of the supported Pt catalysts. A small difference in the catalyst structure may cause a big error in the comparative studies for the size effect. Therefore, there are still too many issues to be investigated for the size effect. 2) the catalyst structure has a great effect on the ORR activity. Higher ORR activities on the high-indexed facets have been observed compared with those on the low indexed ones. The challenges are how to fabricate the catalyst with such high-indexed facets and how to stabilize them. 3) the controlled synthesis of Pt NPs with both control of the size and structure must be a very important future direction. A significant challenge has to be faced: to make a better synthetic control, one may have to consider the alternatives to the conventional carbon supporting materials. Many functional groups in these carbon supports cannot be easily to be controlled and have a significant effect on the Pt nano particle size and structure. The present way to make carbon support is not in a controllable way. New carbon materials with clear frameworks and well-defined structures(including molecular structures and porous structures) must be used. Graphene should be such kind of new carbon materials.135,136However, there is still no ideal graphene commercially available. Many defects or impurities exist in the graphene from the present fabrication. In this regard, one may consider some novel carbon precursors, like porous organic polymers.137,138 Under certain carbonization condition, well-defined carbon support would be available in the near future.137 Right now, well defined synthesis of platinum NPs has been available.56,139 If well-defined carbon support with designable high surface area, desired porous structure, designable high conductivity and controllable anti-corrosion would be available, it must be very helpful for the understanding the ORR mechanism and for the practical applications. 4) among various Pt based catalysts exploited,

shell-core Pt NPs show the most significant potential as ORR catalysts because of their balance between activity and stability. A bulk production of this kind of Pt based catalysts is a significant challenge. 5) the nucleation and crystal growth of the Pt NPs have to be further investigated. The reduction methodologies or the reducing agent has a remarkable influence on the nucleation of Pt NPs. However, the thermodynamic and kinetic of nucleation of Pt NPs are still not clear.

Normally, a slow nucleation occurs with the reduction thermally and chemically. This induces a difficulty in the size and structure control. Recently, a room temperature electron reduction has been employed to induce a fast nucleation of noble metal NPs.93,140,141The obtained Pt and other noble metal NPs always show (111)plane as the principal facet.93,141 Such electron reduced Pt/catalyst has shown enhanced activity and stability for ORR.93 6) *in Situ* catalyst characteristic is still not available for ORR studies. The detection of chemical intermediates is still impossible, which makes the mechanism study very difficult.

2.3 Development of metal free electro catalyst for ORR

As well as identifying and interpreting the active sites and catalytic processes of ORR on the electrocatalytic electrodes, unfolding the microscopic scaling relationship and volcanic trend with the doped elements are much more objective to provide a theoretical guide for experimental synthesis to search the optimal ORR materials in practical application.The key issue, herein, is how to define a catalytic descriptor bridging the electronic properties, the adsorption behaviors of intermediates at RDS and the final catalytic performance. The *d*-band center, as a classical activity descriptor in metal catalysts, hasal ready be used to elucidate the ORR activity. The oxygen-contained species (OH_x, x=0, 1)have been verified as correlating with the *d*-band center of the pure metal surface.127Furthermore, there is a volcanic trend with the corresponding ORR activity in which Pt with a balanced oxygen binding energy is predicted to be closest to the activity peak51. The position of *d*-band center of metal catalysts can be further tuned through alloying. Previous DFT calculations have driven high-throughput screening that the ORR catalytic activity of polycrystalline Pt3Y is enhanced to 6~10 times higher than that of pure Pt catalyst, which has also been successfully verified by experimental characterization. In metal-free materials, the adsorption free energy ΔGOOH and ΔGOH are recognized as the optimal descriptor for the 4e- and 2e- ORR in fuel cells, respectively, which is the origin of the large over potential of ORR on various electrocatalysts, and the *p* orbital of atoms inactive sites are prone to hybridize with ORR intermediate OOH and OH. As analogous to the *d*-band model, Sinthika et al. proposed pz orbital occupancy (OpZ) and the density of state sat the Fermi level projected on pz orbital of

the active sites (DpZ) as electronic descriptors, by which they predicted that the carbon atom lying in the para positions with respect to 3Ndopants exhibits the highest catalytic activity in N/B-doped graphene. From the perspective of natural bond order, the adsorption of ORR intermediates involved the chemical bond formation and the increased filling of antibonding state in the adsorbed species could destabilize the graphene-adsorbate interaction, accordingly leading to the linear relationship between and the lowest valence orbital level revealed of doped graphene cluster.132 This idea is also applicable to analyze the X-doped fullerenes among which their performances are related to the order of ionization potential and the HOMO-LUMO gap. Among the doping systems, the electronegativity difference will break the electronic symmetry in doped materials, triggering the electron redistribution and creating Lewis acid/basic sites. The positive charge atoms (Lewis acid sites) are recognized as the active centers for catalyzing ORR. Zhao et al. introduced a dimensionless parameter to describe this relationship based on the electron electronegativity and electron affinity. It is found that the electronegativity and the electron affinity should also follow the Sabatier principle due to the competition of electron transfer between forming covalent bond and electro-catalytic reaction. The best catalysts should have a balanced electronegativity . electron affinity (a little higher than the carbon atom), which will reduce the over potential of ORR and stabilize the adsorption of intermediates. The work of Zhao et al. declaims that doping near the edge of graphene nano ribbons is a promising strategy in developing highly active metal-free carbon-based catalysts for ORR in both fuel cells and metal–air batteries. For computational work on Li-O_2 batteries, the binding energy of Li_xO_x species and insertion energy of Li in Li_xO_x species were used to make correlation with the catalytic activity of metal-free catalysts,54 which shows similar regulations with the investigations on Pt-based bimetallic catalysts.125 However, there still lacks of systematical theoretical investigations on the more natural properties. Thus, unraveling the structure-activity relationship to bridge experimental and theoretical work still needs a complete catalytic descriptor containing detailed atomic geometric and electronic information. Considering the development of mature database construction and accurate computational methods, designing catalytic descriptor based on burgeoning machine-learning method could be a potential way to correlate the experimental activity and theoretical quantities. Some successful research examples134, 135 on catalyst design are making this more and more practical.

2.4 Applications of electro catalyst for ORR

2.4.1 Li-O_2 batteries :

From the view of computational simulations, most of the publications focus at the cathode catalysts in non-aqueous Li-O_2 batteries, which was first proposed by Abraham andJiang.43 Thus for clarity, all the Li-O_2 batteries referred in the following parts denote the non-aqueous one. Similarly, the fuel cells mentioned afterwards denote the H_2-O_2 fuel cell. The electro-catalytic discharge in cathode can also be view as ORR catalysis, with the reaction medium changes from H+/H_2O into Li+. The Li-O_2 battery is similar to conventional Li-ion battery in configuration, where Li salt is dissolved in aprotic solvents as electrolytes. In the cathode, Li-O_2 batteries use oxygen molecule directly from air as a cathode material, and the composites consist of porous carbon and catalyst act as the lithium oxide substrate, while Li metal is used as the anode and plays a role as the Li source in Li-O_2 battery.44 As illustrated, the two-phase diagram of Li-O_2 discharge process in non-aqueous electrolyte reveals the interface reactions on cathode catalysts. Firstly, oxygen molecules dissolve in the electrolyte, and diffuse on the surface of cathode catalyst together with Li+ from the anode. Then electrons transported in cathode facilitate the reaction between O_2 and Li+ and lead to the formation of the final discharge products (Li oxides), which are insoluble in the electrolyte and will precipitate on the surface of cathode catalyst.45 This provides a useful indicator for theoretical simulations to judge whether the ORR could take place by calculating the charge value on Li oxides. If the adsorbed Li oxides carry negative charge, indicating that O_2 obtains electrons from the cathode catalyst, this meets the requirement of ORR .

facilitates the discharge process in cathode. Similar with ORR occurred in fuel cells, ORR in discharge process of Li-O_2 batteries also presents four-electron and two-electron pathways, which is determined by the involved electron number. Experimentally, the discharge products are insoluble solid lithium peroxide (Li_2O_2) or lithium oxide (Li_2O).46 And the overall reaction equation can be expressed as following:28, 43, 46, 47

$$4Li+ + 4e- + O_2 \rightarrow 2Li_2O (E0 = 2.96 vs.\ Li+/Li) \quad (3)$$

$$2Li+ + 2e- + O_2 \rightarrow Li_2O_2 (E0 = 2.91 vs.\ Li+/Li) \quad (4)$$

Summarized from previous theoretical simulations, there are three reaction mechanisms for initial nucleation of Li_2O_2 in non-aqueous Li-O_2 batteries depending on the initial step a. The Li binding mechanism. For cathode catalysts with Li adsorption preferred first, the Li atom first binds to the active site and provides a binding site for O_2 molecule to form a

LiO_2 group. Such kind of cathode catalyst is always inactive for O_2 adsorption, for instance, some kinds of defective graphene,50 and defect-contained N-doped graphene48.

b. The O_2 associated mechanism. For the cathode catalysts with O_2 adsorption preferred first, the Li atom binds on the adsorbed O_2 and then forms a LiO_2 group. This pathway works on most kinds of cathode catalysts. The O_2 dissociation mechanism. Similar with ORR in fuel cells, the adsorbed O2 may easily dissociate into adsorbed O, most of such kind of cathode catalysts contain rich active sites for O_2 adsorption.

Computationally, the preference of pathway a or b is determined by calculating the adsorption energy of Li/O_2 on substrate.48 After the confirmation of initial nucleation of Li_2O_2,there are still two independent pathways for the further reduction of O_2, involving whether another O_2 molecule will be involved in the as-grown Li_2O_2 cluster, two possible discharge products (Li_2O or Li_2O_2) are formed. A brief illustration of ORR in Li-O_2 batteries is shown in Scheme 2. During the simulation process, the choice of four-electron or two-electron pathway is actually determined by the binding site and free energy changes.

2.4.2 Fuel cells :

The overall reaction equation in H_2-O_2 fuel cells can be expressed by $2O_2 + 2H_2 \rightarrow 2H_2O_2$ microscopic mechanism of this simple reaction is still elusive in the electro-catalysis. The concrete reaction pathway of ORR, involving multi-electron transfer and multi-step processes, is relevant to the electrolyte media. PEMFCs in acid environment attract much more academic and industrial interests due to the successful commercialization of the protonex change membrane (PEM). However, various non precious catalysts show better performance in the alkaline media due to the media effect on the adsorption ofintermediates.36, 37 And the first fuel cell that was ever put to practical use is the alkaline fuel cell operated by NASA.38 In acid conditions, the successive protonation of oxygen into water is the main mechanism of electro-catalytic reduction. Under alkaline conditions, water (H_2O) moleculesare not only as a solvent, but also as a reactant to provide protons and participate in reacting with O_2, releasing hydroxyl radical (OH-). Two main possible mechanisms could happen, namely, oxygen dissociative mechanism by forming dissociated O atoms or associative mechanism through forming peroxyl (OOH):a. O_2 dissociation mechanism. For the cathode catalysts with strong O_2 adsorption, O_2 may dissociate into adsorbed O firstly due to the low dissociation barrier, followed by the pronation into *OH or reacting with water into 2OH-.b. O_2 association mechanism. After O_2 adsorption, O_2 combines (H++e-) or reacts withH_2O into *OOH firstly. Then O-O bond tends to dissociate

into H_2O or OH-, leaving *O. Finally, the adsorbed oxygen atom shares the similar O_2 dissociation step, and will be hydrogenated into H_2O or OH- at acid or alkaline conditions. Four-electron pathway (4e-) of oxygen into water is the most ideal high-rate reaction pathway without generating extra byproducts. However, there still exists a chance to produceH_2O_2 during ORR through two-electron (2e-) process in the O_2 association mechanism, in which H_2O_2 may corrode the catalysts surface due to its strong oxidizability. Then H_2O_2 may further react with two electron-proton pairs into H_2O or dissociate into water and oxygen. It should be noted that the aforementioned reaction pathways shown in Scheme 1 are mainly the inner-sphere electron transfer (ISET) processes happened in the inner-Helmholtzplane (IHP) where the ORR reactants need to connect to the surface of catalysts during an elementary reaction, denoted ISET@IHP mechanism. However, it is revealed that the experimental exchange current density values in alkaline media is independent on some electrode materials, including silver, gold, manganese oxides, perovskites, and various carbon surface.39 The outer-sphere electron transfer (OSET) mechanism accounts for this surface-independent phenomenon. Under alkaline conditions, the original over potential of $O_2 + e- \rightarrow O_2-$could decrease from 1.53 V at pH=0 to 0.7 V at pH=14 due to the effect of pH, the solvated molecular O_2 tends to pre-activate, forming O_2-or $OOH-$through electron transfer (ET) from the electrode surface with the help of weak hydrogen bonding.40 Then the pre-activatedO_2-in alkaline environment could react with H_2O into OOH- and OH- .

2.3 CONTEMPARORY RESEARCH:

2.3.1 Nitrogen doped carbon nanotubes as Metal-Free Catalysts for ORR :

Apart from their use as noble-metal-catalyst supports described in section 3.1.2, aligned CNTs formed by high-temperature treatment of certain metal heterocycle molecules (e.g.,ferrocene/NH_3) were demonstrated to show some ORR electrocatalytic activities in 2008.261 However, the observed electrocatalytic activity was attributed to the presence of FeN_2−C and/or FeN_4−C active sites in the nanotube structure containing Fe residues.261 Similarly, N-doped carbon fibers (CNFs), prepared by pyrolysis of FePc, have been demonstrated to show electrocatalytic activities for ORR via a two-step two-electron pathway.262 The N-doped CNFs showed an over 100-fold increase in catalytic activity for H_2O_2decomposition in both neutral and alkaline conditions,263 albeit still less electroactive than the Pt catalyst. The observed ORR activities were attributed to the presence of the Fe−N_2

activesites bound to carbon support and/or the exposed edge plane defects coupled with nitrogen doping to influence adsorption of reactive intermediates.262 Although the N doping has greatly improved the ORR activity, these noble-metal-free catalysts still exhibited poorer, or at the best comparable, ORR performance with respect to Pt catalysts and many even with a two-step, 2e−pathway. It was the discovery of the efficient electrocatalytic activity for metal-free VA-NCNTs with a 4e− ORR process(Figure 13)8 that opened an entire field of metal-free carbon electrocalaysts. Since then, numerous methodologies have been developed for preparing metal-free ORR electrocatalysts base don heteroatom-doped CNTs, graphene sheets, and/or graphite nanoparticles.

As mentioned above, the CVD processes for producing the NCNTs used as metal-free catalysts often involve metal residues (e.g., Fe),8 and considerable care has been taken during electrode preparation to completely remove the catalyst residue. However, possible effects of metal contaminates on then observed superb ORR performance could still be a matter of controversy unless nitrogen-doped carbon materials with excellent ORR electrocatalytic activities can be produced by a metal-free preparation procedure. In this regard, Dai and coworkers developed a simple plasma etching technology to effectively generate metal-free catalysts from efficient metal-free growth of single-walled NCNTs. Although the metal-free growth of CNTs reported independently by Liu et al. and Huang et al. offered an alternative approach to metal-free CNTs attractive for many existing and new applications, including ORR, the possible use of those nitrogen-free CNTs produced by the metal-free growth has been largely precluded by its low growth efficiency. In order to enhance the metal free growth yield of CNTs, Yu et al. developed a simple but effective approach to the growth of densely packed undopedand/or nitrogen-doped SWCNTs from metal-free nanoparticles produced by water-plasma etching SiO_2/Si wafers. atomic force microscope(AFM) imaging of the water-plasma-etched SiO_2/Si substrate clearly shows the formation of homogeneously distributed catalyst particles with an average size of <5 nm. The particle density was estimated to be ∼150 particles/μm2. Prior to nanotube deposition, XPS was used to confirm that the water plasma-induced nanoparticles, with and without HNO_3 washing, are free from metal. The metal-free SiO_2 nanoparticles were demonstrated to effectively support the growth of CNTs under a mixture flow of 100 sccm CH4 and 100 sccm H_2 at 900 °C for 20min (Figure 18B(c)). Similarly, it was found that CNTs can also effectively grow on the water-plasma-etched quartz and mica surfaces, indicating the versatility of the plasma etching for creating high-density metal-free catalyst particles on various substrates. By introducing 50 sccm NH_3 during the metal-free CVD process, densely packed NCNTs were produced on the water-plasma-etched SiO_2/Si substrate . In contrast, no

nanotube deposition was seen for the pristine SiO_2/Si wafer under the same condition. High-resolution transmission electron microscopy (HRTEM) observation reveals single-wall characteristics , which was further supported by Raman spectra showing the radial breathing modes (RBM) of SWCNTs. The RBM peaks at 150.7, 170.0, 179.6, and 192.7cm−1 correspond to nanotube diameters of 1.65, 1.46, 1.38, and1.29 nm, respectively,276 largely consistent with the electron microscopic observation. The corresponding XPS spectraclearly indicate the absence of any metal element for either CNTs or NCNTs produced by the metal-free growth. XPS N 1s spectrum for the NCNTs (3.6 atom % N),together with the curve fitting, given in, reveals two peaks at about 401 and 398 eV attributable to the pyrrolic(17%) and pyridinic (83%) nitrogen, respectively, with the pyridine nitrogen being dominant. This is an addition advantage for the metal-free NCNTs to be used for ORR as the pyridinic group has been shown to be more active than its pyrrolic counter part. Compared with undoped CNTs, the metal-free NCNTs were indeed demonstrated to show relatively good electro catalytic activity and long-term stability toward ORR even in an acidic medium. As seen in Figure 19a, the NCNT/GC electrode showed a substantial reduction process at about 0.2 V in the presence of oxygen, while no obvious response was observed at the same potential range under N2. Compared to CNTs, the ORR onset potential for the NCNTs shifted to a more positive value with a considerably higher electrocatalytic activity . A first-order reaction was found for reduction of the dissolved oxygen. The electron transfer number (n) for the NCNTs was derived to be 3.52−3.92 at potential ranging from−0.1 to 0.2 V, suggesting a four-electron process for the ORR on the NCNT electrode . The continuous potential cycling did not cause any loss of the specific catalytic activity for the NCNT electrode , indicating that the catalytic sites of the NCNT were rather stable even in an acidic medium. Owing to the highly generic nature characteristic of the plasma etching technique, the plasma-enhanced metal-free CVD can be applied to many other substrates for efficient growth of metal free CNTs useful for various applications, ranging from energy related to electronic systems.

Nitrogen doping has been widely used to modulate the electronic properties of carbon nanomaterials and found to significantly influence oxygen reduction, hydrogen peroxide decomposition, and alcohol oxidation reactions.287 Generally speaking, the introduction of nitrogen atoms as do pants into CNTs perturbsthe homogeneous π-electron cloud to change the electronic surface state of the CNT,288 which often increases its chemical activity and electron conductivity.289 Tunneling microscopy and theoretical calculations have shown that N doping of CNT increases the Fermi energy to facilitate electrons to reach the conduction band to exhibit metallic properties.289 The observed increase in the localized density of states at the Fermi level could cause considerable electron emissions at sufficiently low

voltages, thereby increasing catalytic activities of carbon directly related to the effect of the nitrogen lone pair electrons on the conjugation of the graphitic π-system. Computer simulations showed that the energy barrier for ORR at a carbon atom could be reduced by the presence of an adjacent nitrogen atom. Of particular interest, Wiggins-Camacho and coworker investigated the influence of nitrogen content in N doped CNTs on the electronic and electrochemical properties and found an increase in bulk electrical conductivity, work function, density of the states at the Fermi level, and ORR activity with increasing nitrogen-doping level. Nitrogen content is the most important factor that should be governed to obtain high catalytic activity. Chen et al. produced NCNTs with varying nitrogen contents through a single-step CVD process. Indeed, these authors found that NCNTs with higher nitrogen content and more defects exhibited better ORR performance even in acidic electrolytes.

2.3.2 Boron-Doped Carbon Nanotubes as electrocatalyst for ORR :

Recent research activities have demonstrated that the N-doping-induced charge transfer mechanism for ORR catalyzed by N-doped carbon nano materials can be applied to the design/development of new metal-free catalytic materials for fuel cell and many otherapplications.76 For instance, Yang et al. recently extended the doping atoms to include boron using boron-doped CNTs(BCNTs) with a tunable boron content of 0−2.24 atom %synthesized by CVD of benzene, triphenylborane (TPB), and ferrocene precursors at different TPB concentrations.17 There sultant BCNTs were subjected to CV testing (Figure 23a). It was found that the maximum peak current, along with the steady state diffusion current and the onset and half-wave potential, increased with increasing boron content from 2.8 (CNTs, 0 atom % B) through 3.2 (B_1CNTs, 0.86 atom % B) and 3.8 (B_2CNTs,1.33 atom % B) to 8.0 mA mg−1 (B_3CNTs, 2.24 atom % B).Besides, a progressive positive shift of the peak potentials with increasing boron content from −0.43 (CNTs) through −0.41-(B_1CNTs) and −0.38 (B_2CNTs) to −0.35 V (B_3CNTs) in reference to the saturated calomel electrode (SCE) was observed (Figure 23a). Furthermore, RRDE measurements revealed that the transferred electron number per oxygen molecule increased slightly from 2.2 for CNTs to 2.5 for B_3CNTs, indicating dominant two-electron ORR process. Like NCNTs, the BCNT catalysts also show an excellent stability and are free from methanol cross-over and CO poisoning. Although the performance of BCNTs is not yet as good as the commercial Pt/catalyst (Figure 23b), the proportional relationship between ORR performance and boron content suggests the great potential of BCNTs for further improvement.4.1.1.5. Role of Boron Doping for ORR. To understand the electrocatalytic activity of BCNTs, DFT calculations were performed on boron-doped armchair (5,5) SWCNT (i.e.,BCNT(5,5)) before and after O_2

adsorption. geometry optimization and the subsequent natural bond orbital(NBO) analysis.17 It was found that B doping induced a transformation of the electron-deficient boron to electron donating site by taking p electrons of the conjugated carbon network. Consequently, the 2pz orbital of the boron atom holds a fraction of lone pair electrons with an amount of 0.51e, which constitutes the main protruding lobe in the highest occupied molecular orbitals (HOMO-1) of BCNT(5,5) (Figure 24a) to act as the electron-donating site for the ORR. The protruding lobe of the spin-down HOMO-1 of BCNT(5,5) will then have maximal overlap with the lowest unoccupied molecular orbital(LUMO) of a triplet O2 (Figure 24b) to form an end-on adsorption (Figure 24c), facilitating the ORR process. As can be seen above, the doping-induced charge redistribution, regardless of whether the do pants have a higher (as N)or a lower (as B) electronegativity than that of carbon (Figure24d), could create charged sites (C+ or B+) favorable for O_2 adsorption to facilitate the ORR process. This suggests further exploration of the metal-free electrocatalysts based on CNTs doped by atoms (other than N and B) with electronegativities different from that of the carbon atom.

2.3.3 P-doped carbon materials as electrocatalyst for ORR

Same as VA-group element with N, phosphorus (P) doping will also trigger the enhancement on ORR catalysis of carbon materials. Liu *et al.* firstly reported that P-doped graphite (P-G) manifested a higher oxygen reduction current density than that of Pt-C electrode in the oxygen-saturated alkaline solution, which is similar to those of the N-doped graphite and N-CNT materials. The ORR enhancement under basic solution was also found in the P-incorporated graphene (P-Gr). P dopant in the carbon lattice acts as a good electron donor with lower electronegativity than N, which will introduce more positive charges for O_2 adsorption. By comparing the near-edge X-ray absorption fine structure (NEXAFS) spectroscopy between experimental observation and theoretical simulation, Shimoyama et al. concluded that the three-coordinated P-Gr with planar π-conjugated carbon were preferentially synthesized under high-temperature doping while it is prone to form curved structure at room temperature. Electrochemical data in acid solution suggest that the curved P-G exhibited remarkable catalytic activity for oxygen-related reduction reactions. Although the exact catalytic site is confirmed, the micro-mechanism of ORR in P-Gr is still in debates due to its complex chemical bonding state. For three-coordinated P (P-3C), the optimized doping structure in graphene matrix is corresponding to the anchored P atom with an out-plane-height of 0.09 Å due to a longer P-C bond length than C-C bond. Then oxygen

molecule tended to adsorb on the P site with the calculated adsorption energy of 1.02 eV. A charge transfer from P to the $2\pi^*$ orbital of O_2 will help decompose O_2 into 2*O with activation barrier of 0.38 eV and the subsequent continuous protonation of *O need overcome a rate-determining barrier of 1.06 eV, which is difficult to surmount at room temperature. The 2e- pathway with the formation of *OOH as the initial state is much more energetically favorable, followed by the broken of O-O bond through 4e- process (*HOO +(H++e-)→H_2O+*O and *O+2(H++e-)→ H_2O).91 The energy barrier of RDS is just 0.88 eV happened at the desorption of the second oxygen specie *OH+(H++e-)→H_2O. Thus the 2e and 4e- pathways is coexisted in the P-Gr, during which is consistent with the number of the transferred electron 3.0~3.8 observed in the experiment.89 For four-coordinated P (P-4C), the P dopant tends to occupy in the divacancy of graphene connected to the C atoms with a planar structure. Compared with the three-coordinated P, P-4C has lower formation energy, thus more easily to form. The optimal reaction pathway in P-Gr is along the pathway of *O_2→*OOH→*O→*OH, whose RDS is the hydrogenation of the single adsorbed OH (*OH+H++e- → *+H_2O) with an energy barrier of around 0.85 eV. However, the calculated Over potential is just 0.27 V under the practical condition, which is lower than the commercial.

Pt-C catalysts.92Except for P-C bonds, it is confirmed that P-O bond can also exist due to the strong oxidation of P. The formation of P-O bonds in the P-3C and P-4C sites were also investigated It is found that P-O, as a sole dopant, has lower formation energy than that of sole P-doped configuration. In the P-3C with P-O bond (OP-3C), it has the most negative formation energy and the highest binding energy, corresponding to the highest feasibility in the experimental realization. Meanwhile, introducing the O atom will saturate the local electronic state of P due to the sp3 hybridization in OP-3C, rendering OP-3C half-metal compared with the original semiconductor in P-3C. Furthermore, the introduction of O will activate the adjacent C atom and the RDS of activation barrier will decrease obviously. In the configuration with P-O bond in the four-coordinated P (OP-4C), ORR activity on the P site exhibited the best free energy diagram along O_2 associative mechanism at the equilibrium potential in P-doped systems. Given the formation energy, binding energy and conductivity and catalytic mechanism, the OP-3G is predicted to be the optimal ORR instead of pristine P-Gr . Thus local chemical configuration in P-doped systems plays a vital role in the ORR catalysis.

2.4.4 A Superior ORR Electrocatalyst Based on rGO and Iron (II) Phthalocyanine Supported Platinum Nanoparticles :

Direct methanol fuel cells (DMFCs) have attracted significant attention for portable power applications due to their distinctive advantages of high energy density and energy conversion efficiency. Other advantages include safe storage and transportation of methanol as a liquid fuel, low pollutant emissions, and simple operation. Catalysts, especially used in oxygen cathode have caught a lot researcher's eyesight. It is highly desired to design catalysts with high oxygen reduction reaction (ORR) activity, long-term stability, anti-poisoning of the crossover methanol from anode region, and cost-effective and ease of control during preparation.

Platinum has been used as a catalyst for oxygen reduction reaction (ORR) at the cathode of DMFCs due to its high specific activity. In recent years, a series of new catalysts have been developed to enhance the performance of ORR, such as Pt atoms, designed Pt nanostructures, multi component Pt alloys, non-precious metal catalysts, organometallic catalysts, metal-free catalysts and carbonaceous-supported Pt NPs. To date, commercial carbon supported Pt NPs (Pt/C) are still the most widely used catalyst for ORR in DMFCs, however, its high cost, poor durability, and variable tolerance to methanol over prolonged operation have to be circumvented before wide spread commercialization of DMFCs can be realized. The catalysts composed of graphene supported Pt NPs were proved to offer considerable improvements due to their large surface area, high electrical conductivity.

unique electron transfer and charge-carrier mobility.24 A newly discovered member of the carbon family, graphene is an attractive candidate for fuel cell application. Graphene is densely packedin a honeycomb crystal lattice with a planar geometry. It is a building block for carbon materials of all other dimensionalities, e.g. 0 dimensional (D) buckyball, 1 D nanotubes, 2 D sheets, and 3D graphite. Importantly, the graphene sheets with sp2 hybridization and 2 D planar geometry will further facilitate electron transfer, due to lowering the activation energy related to the ORR.25Compared with carbon nanotubes and other carbon supports, the graphene displays high electrical conductivity (106 S cm-1), thermal conductivity (5,000 W m-1 k-1), fracture strength(124 GPa), specific surface area (2,630 m2 g-1) and charge mobility (105 cm2 V-1 s-1), and low density (1 g cm-3), which ensure graphene as a more effective catalyst support to improve electrochemical reactivity of DMFCs. However, the susceptibility to oxidative environments,the limited capacitance, and toxic qualities hindered applications of the pure graphene sheets despite the above physical property advantages. It was found that graphene nanocomposites are more practical for

diversified applications, such as solar energy and fuel cells, due to lower material usage, limiting potential toxicity and oxidation. Recent studies indicated that graphene can provide a platform to produced nanocomposites as catalysts by controllable functionalization. Different approaches have been investigated to functionalize graphene and to create building blocks with unique structures. These methods include chemical covalent and noncovalent modification, galvanic replacement, electroless deposition, hydrothermal and solvothermal growth to tune the functionality of graphene sheets in reduced form, which can be utilized based on the end-user application.N4-chelate complex with transition metals was first reported as catalysts to be used in oxygen electrochemical reduction in 196442. Many works focus on the M-N4 towards their ORR catalyticproperty43,44. The ferrous Iron (II) phthalocyanine (FePc) was believed with the best performance among these M-N4 ORR catalyst 45. Although effort has been made for FePc in the usage of ORR catalyst, they cannot reach the level of Pt-based catalyst both in reactivity and durability .

The metal phthalocyanine (MPc) was chosen due to its property of tolerance to methanol and availability of an electron sink due to bond in the conjugated ring system. The aggregation of FePc molecular and the poor electron conductivity hinder its application in ORR . Different carbon materials, for example, Vulcan XC-7248 and carbon nanotubes were used as a support for MPc. Reduced graphene oxide (rGO) was selected as support and MPc as a mediator agent to construction graphene building blocks.50,51 The conjugation between delocalized π-electrons within MPc and p-electron within the carbon atom from rGO will be one of the important factors to determine the redox properties of these composite. The characteristic of MPc, such as aromatic macrocyclic with nitrogenous functional groups allows for its conjugation with graphite surface structure of rGO. It was found that phthalocyanines act as planar tetradentate dianionicligands to coordinatively bind with metal centers through “four inwardly projecting nitrogen centers”, leading to the common term “transition metal N4 macrocycles”. The ferrousIron (II) phthalocyanine (FePc) is a widely studied porphyrin-like molecule, which displays a strong tendency to axial ligation. The ferrous phthalocyanine (FePc) among the MPc series was implemented due to its flexibility and ability of electron transfer from Fe (II) d-orbital to the ligands. It is hypothesized that the phthalocyanine as an aromatic organic molecule can strongly interact with graphene via π-π stacking. rGO or N doped rGO supported FePc are normally used as the ORR catalysts in an alkaline system. Graphene oxide (GO) supported FePccould be applied in the aqueous system close to neutral 60 and even the binuclear iron (III)phthalocyanine graphene nanosheets could be used in acidic solution.61In this work, we aim to develop a simple and feasible synthetic route to produce cost-effectiveand robust electrocatalysts with tunable structure and excellent

stability. A “Suspension Unit for Reactive Evolution ” method was developed to prepare Pt/FePc@rGO catalysts, which showed uniform nanostructure and superior electrochemical performance. Even some researcher shave investigated the FePc/rGO electrocatalysis properties, but the low current density can still not reach the level of Pt base catalysts. Although some attempts to prepare Pt NPs and GO sheet composite, most of them only focus on the electrocatalysis properties in acidic solutions, a few of them show a light on the basic solution systems, let alone studying the effects in methanol and alkaline system. The catalyst prepared by ***SURE*** method shows good properties in alkaline system and methanol tolerant property as well. Due to the high electrical conductivity of rGO, the d electron of Fe2+ with the Pc unit electrons (ē) transfer to rGO is thermodynamically favourable when FePc is combined with rGO. Therefore, the FePc will be ‘electron deficient’ to attract ē from Pt in PtCl42- (using the K2PtCl4 salt) and then the PtCl42- will be reduced to Pt byH2 to achieve a uniform loading of a metal catalyst. Pt/FePc@rGO catalyst shows a high ORR activity, long time stability, and anti-poisoning property towards the crossover of methanol in analkaline system.

2.3.5 TiO_2/rGO composite as electro catalyst for ORR

Proton exchange membrane fuel cells (PEMFCs) are viewed as promising energy conversion devices for future sustainable energy generation applications due to their high conversion efficiency and power density.1,2 Although platinum-based nanomaterial shave been regarded as the most effective electrocatalysts toward the ORR, these materials still suffer from scarcity, high cost, low stability and low methanol tolerance.3–5 Many efforts have recently been devoted to the preparation of metal-free and non-precious metal catalysts, including B-, N- and S-doped.

Carbonmaterials, transitionmetal chalcogenides, transitionmetal carbides and transition metal oxides.6–15Among various non-precious oxide catalysts, TiO_2 is considered as a suitable candidate because of its low cost, high electron conductivity, and high activity. Recently, some experimental research studies proved that TiO_2-based composites exhibit catalytic properties.16–21 Jiemei Yu et al.22 reported the synthesis of a reduced graphene oxide (rGO) supported (N,F)-co-doped amorphous TiO_2 composite (TiO_2/rGO) by one-pothydrolysis as well as its electro-activity toward the ORR in analkaline electrolyte. XPS showed that the N and F dopants inhibited the growth of the TiO_2 crystals and promoted the formation of anatase TiO_2. Hao Cheng et al.23 found that the two step hydrothermal synthesis of

Co/TiO_2/C–N and its enhanced ORR activity in a 0.1 M KOH solution. The results show that the proper addition of a transition metal (Co) significantly creates more active sites and improves the ORR activity. Yuewu Zhaoet al.24 revealed that a titanium dioxide/graphene support edhemin (TiO_2/Gr/Hem) composite was successfully prepared through a two-step solvo thermal reaction, and it exhibited electro catalytic activity toward the ORR in alkaline media. The high ORR activity was mainly attributed to the increased structural defects, active sites, geometrical complexity, pyridinic N, pyrrolic N, and the inhibitory effect of TiO_2 on hydrogen peroxide. It was revealed that the catalytic activity for the ORR can be further enhanced through the combination of TiO_2 and hemin. It is generally observed that crystals with different types of exposed facets usually exhibit different physical and chemicalproperties.25 Yihe Zhang et al.26 found that cubic-shaped Co_3O_4nanocrystals with a size of 9 nm (Cubic-9/C) exhibited a better ORR catalytic activity than Cubic-18 and Triangular-9 in alkaline solution. It was mainly attributed to the large specific surface area and the optimal concentration of oxygen vacancies inCubic-9. These results open up a new route for the rational design of non-noble metal catalysts for energy conversion applications. Although some works on the synthesis and catalytic activity of TiO_2 nanocrystals have been reported, investigation concerning the effect of different TiO_2 morphologies on electrocatalytic properties toward the ORR remains a challenge and is worth further exploration.

2.4 References

1. Z. Chen, D. Higgins, A. Yu, L. Zhang and J. Zhang, *Energy Environ. Sci.*, 2011, **4**, 3167-3192.

2. F. Cheng and J. Chen, *Chem. Soc. Rev.*, 2012, **41**, 2172-2192.

3. R. Padbury and X. Zhang, *J. Power Sources*, 2011, **196**, 4436-4444.

4. B. Wang, *J. Power Sources*, 2005, **152**, 1-15.

5. H. A. Gasteiger and N. M. Markovic, *Science*, 2009, **324**, 48-49.

6. M. Armand and J. M. Tarascon, *Nature*, 2008, **451**, 652-657.

7. Y. Wang and P. B. Balbuena, *J. Phys. Chem. B*, 2005, **109**, 14896-14907.

8. Y. Sha, T. H. Yu, Y. Liu, B. V. Merinov and W. A. G. III, *J. Phys. Chem. Lett.*, 2010, **1**, 856-861.

9. G. Wei, Y. Fang and Z. Liu, *J. Phys. Chem. C*, 2012, **116**, 12696-12705.

10. N. M. MarkovicÂ, T. J. Schmidt, V. StamenkovicÂ and P. N. Ross, *Fuel Cells*, 2001, 105-116.

11. J. A. Keith and T. Jacob, *Angew. Chem. Int. Ed.*, 2010, **49**, 9521-9525. 12. J. A. Keith, G. Jerkiewicz and T. Jacob, *ChemPhysChem*, 2010, **11**, 2779-2794.

13. V. Tripkovic, E. Skulason, S. Siahrostami, J. K. Norskov and J. Rossmeisl, *Electrochim. Acta.*, 2010, **55**, 7975-7981.

14. S. Suzuki, T. Onodera, J. Kawaji, T. Mizukami and K. Yamaga, *Appl. Catal. A-Gen.* , 2012, **427**, 92-97.

15. Z. W. Liu, F. Peng, H. J. Wang, H. Yu, C. L. Chen and Q. Q. Shi, *Catal. Commun.*, 2012, **29**, 11-14.

16. M. J. Janik, C. D. Taylor and M. Neurock, *J. Electrochem. Soc.*, 2009, **156**, B126-B135.

17. M. Winter and R. J. Brodd, *Chem. Rev.*, 2004, **104**, 4245-4269.

18. C. Sealy, *Mater. Today*, 2008, **11**, 65-68.

19. K. Gong, F. Du, Z. Xia, M. Durstock and L. Dai, *Science*, 2009, **323**, 760-764.

20. L. Dai, Y. Xue, L. Qu, H. J. Choi and J. B. Baek, *Chem. Rev.*, 2015, **115**, 4823-4892.

21. Z. Yang, Z. Yao, G. Li, G. Fang, H. Nie, Z. Liu, X. Zhou, X. Chen and S. Huang, *ACS Nano*, 2012, **6**, 205-211.

22. S. Zhao, J. Liu, C. Li, W. Ji, M. Yang, H. Huang, Y. Liu and Z. Kang, *ACS Appl. Mater. Inter.*, 2014, **6**, 22297-22304.

23. K. Zhou, W. Zhou, X. Liu, Y. Wang, J. Wan and S. Chen, *ACS Appl. Mater. Inter.*, 2014, **6**,

14911-14918.

24. X. Wang, J. Wang, D. Wang, S. Dou, Z. Ma, J. Wu, L. Tao, A. Shen, C. Ouyang, Q. Liu and S. Wang, *Chem. Commun.*, 2014, **50**, 4839-4842.

25. Z. L. Ma, S. Dou, A. L. Shen, L. Tao, L. M. Dai and S. Y. Wang, *Angew. Chem. Int. Ed.*, 2015, **54**, 1888-1892.

26. S. Chen, J. Y. Bi, Y. Zhao, L. J. Yang, C. Zhang, Y. W. Ma, Q. Wu, X. Z. Wang and Z. Hu,

Adv. Mater., 2012, **24**, 5593-5597.

27. H. L. Jiang, Y. H. Zhu, Q. Feng, Y. H. Su, X. L. Yang and C. Z. Li, *Chem. Eur. J.*, 2014, **20**, 3106-3112.

28. G. Girishkumar, B. McCloskey, A. C. Luntz, S. Swanson and W. Wilcke, *J. Phys. Chem. Lett.*, 2010, **1**, 2193-2203.

29. Y. Shao, S. Park, J. Xiao, J. Zhang, Y. Wang and J. Liu, *ACS Catal.*, 2012, **2**, 844-857.

30. M. M. Montemore, M. A. van Spronsen, R. J. Madix and C. M. Friend, *Chem. Rev.*, 2018, **118**, 2816-2862.

31. K. M. Ervin, I. Anusiewicz, P. Skurski, J. Simons and W. C. Lineberger, *J. Phys. Chem. A*,

2003, **107**, 8521-8529.

32. B. Ruscic, R. E. Pinzon, M. L. Morton, N. K. Srinivasan, M.-C. Su, J. W. Sutherland and J. V. Michae, *J. Phys. Chem. A*, 2006, **110**, 6592-6601.

33. B. B. Blizanac, P. N. Ross and N. M. Markovic, *Electrochim. Acta.*, 2007, **52**, 2264-2271.

34. K. Kato, T. Uda and K. Terakura, *Phys. Rev. Lett.*, 1998, **80**, 2000-2003.

35. A. Ziletti, A. Carvalho, D. K. Campbell, D. F. Coker and A. H. Castro Neto, *Phys. Rev. Lett.*, 2015, **114**, 046801.

36. J. S. Spendelow and A. Wieckowski, *Phys. Chem. Chem. Phys.*, 2007, **9**, 2654-2675.

37. X. Ge, A. Sumboja, D. Wuu, T. An, B. Li, F. W. T. Goh, T. S. A. Hor, Y. Zong and Z. Liu,

ACS Catal., 2015, **5**, 4643-4667.

38. P. Quaino, N. B. Luque, R. Nazmutdinov, E. Santos and W. Schmickler, *Angew. Chem. Int.*

Ed., 2012, **51**, 12997-13000.

39. R. Nagappan and M. Sanjeev, *J. Phys. Chem. C*, 2011, **115**, 18015-18026.

40. R. Nagappan and M. Sanjeev,*Advances in Physical Chemistry*, 2012, **2012**, 1-17.

41. A. Ignaczakd, R. Nazmutdinovc, A. Goduljana, L. M. de C. Pintoa, F. Juareza, P. Quainoe,

E. Santosa and W. Schmicklera, *Nano Energy*, 2016, **29**, 362-368.

42. H. Shi, Y. Shen, F. He, Y. Li, A. Liu, S. Liu and Y. Zhang, *J. Mater. Chem. A*, 2014, **2**, 15704-15716.

43. K. M. Abraham and Z. Jiang, *J. Electroanal. Chem.*, 1996, **143**, 1-5.

44. J. S. Lee, S. T. Kim, R. Cao, N. S. Choi, M. Liu, K. T. Lee and J. Cho, *Adv. Energy Mater.*,
2011, **1**, 34-50.

45. Z. Y. Wen, C. Shen and Y. Lu, *ChemPlusChem*, 2015, **80**, 270-287.

46. M. D. Radin, J. F. Rodriguez, F. Tian and D. J. Siegel, *J. Am. Chem. Soc.*, 2012, **134**, 1093-1103.

47. J. Read, *J. Electrochem. Soc.*, 2002, **149**, A1190-A1195.

48. Y. Jing and Z. Zhou, *ACS Catal.*, 2015, **5**, 4309-4317.

49. H. J. Yan, B. Xu, S. Q. Shi and C. Y. Ouyang, *J. Appl. Phys.*, 2012, **112**, 104316.

50. H. R. Jiang, P. Tan, M. Liu, Y. K. Zeng and T. S. Zhao, *J. Phys. Chem. C*, 2016, **120**, 18394-18402.

51. J. K. Nørskov, J. Rossmeisl, A. Logadottir, L. Lindqvist, J. R. Kitchin, T. Bligaard and H. Jo´nsson, *J. Phys. Chem. B*, 2004, **108**, 17886-17892.

52. Y. Jia, L. Zhang, A. Du, G. Gao, J. Chen, X. Yan, C. L. Brown and X. Yao, *Adv. Mater.*, 2016, **28**, 9532-9538.

53. U. Ryde, *Med. Chem. Commun.*, 2014, **5**, 1324-1336.

54. H. Dong, Y. Ji, T. Hou and Y. Li, *Carbon*, 2018, **126**, 580-587.

55. F. G, L. Ferrighi and C. V. Valentin, *J. Catal.*, 2014, **318**, 203-210.

56. T. A. Halgren and W. N. Lipscomb, *Chem. Phys. Lett.*, 1977, **49**, 225-232.

57. G. Henkelman and H. Jonsson, *J. Chem. Phys.*, 2000, **113**, 9978-9985.

58. G. Henkelman, B. P. Uberuaga and H. Jonsson, *J. Chem. Phys.*, 2000, **113**, 9901-9904.

59. F. Banhart, J. Kotakoski and A. V. Krasheninnikov, *ACS Nano*, 2011, **5**, 26-41.

60. C. Tang, H. F. Wang, X. Chen, B. Q. Li, T. Z. Hou, B. Zhang, Q. Zhang, M. M. Titirici and F. Wei, *Adv. Mater.*, 2016, **28**, 6845-6851.

61. Y. Jiang, L. Yang, T. Sun, J. Zhao, Z. Lyu, O. Zhuo, X. Wang, Q. Wu, J. Ma and Z. Hu, *ACS Catal.*, 2015, **5**, 6707-6712.

62. Q. Ly, B. V. Merinov, H. Xiao, W. A. Goddard and T. H. Yu, *J. Phys. Chem. C*, 2017, **121**,
24408-24417.

63. T. Ikeda, Z. Hou, G. L. Chai and K. Terakura, *J. Phys. Chem. C*, 2014, **118**, 17616-17625.

64. V. V. Chaban and O. V. Prezhdo, *J. Am. Chem. Soc.*, 2015, **137**, 11688-11694.

65. D. Kwak, A. Khetan, S. Noh, H. Pitsch and B. Han, *ChemCatChem*, 2014, **6**, 2662-2670.
66. H. Wang, T. Maiyalagan and X. Wang, *ACS Catal.*, 2012, **2**, 781-794.
67. W. A. Saidi, *J. Phys. Chem. Lett.*, 2013, **4**, 4160-4165.
68. J. Zhang, Z. Wang and Z. Zhu, *J. Mol. Model*, 2013, **19**, 5515-5521.
69. M. Li, L. Zhang, Q. Xu, J. Niu and Z. Xia, *J. Catal.*, 2014, **314**, 66-72.
70. W. Liang, J. Chen, Y. Liu and S. Chen, *ACS Catal.*, 2014, **4**, 4170-4177.
71. H. Kim, K. Lee, S. I. Woo and Y. Jung, *Phys. Chem. Chem. Phys.*, 2011, **13**, 17505-17510. 72. X. Hou, Q. Hu, P. Zhang and J. Mi, *Chem. Phys. Lett.*, 2016, **663**, 123-127.
73. M. Kaukonen, R. Kujala and E. Kauppinen, *J. Phys. Chem. C*, 2011, **116**, 632-636.
74. D. Srivastava, T. Susi, M. Borghei and L. Kari, *RSC Adv.*, 2014, **4**, 15225-15235.
75. X. Chen, J. Chang and Q. Ke, *Carbon*, 2018, **126**, 53-57.
76. S. Dou, A. Shen, L. Tao and S. Wang, *Chem. Commun.*, 2014, **50**, 10672-10675.
77. M. Jiao, W. Song, K. Li, Y. Wang and Z. Wu, *J. Phys. Chem. C*, 2016, **120**, 8804-8812.
78. T. Fukushima, W. Drisdell, J. Yano and Y. Surendranath, *J. Am. Chem. Soc.*, 2015, **137**, 10926-10929.
79. N. D. Ricke, A. T. Murray, J. J. Shepherd, M. G. Welborn, T. Fukushima, T. V. Voorhis and Y. Surendranath, *ACS Catal.*, 2017, **7**, 7680-7687.
80. H. Zhang, J. Zhao and Q. Cai, *Phys. Chem. Chem. Phys.*, 2016, **18**, 5040-5047.
81. K.-H. Yun, Y. Hwang and Y.-C. Chung, *J. Power Sources*, 2015, **277**, 222-227.
82. J. H. Lee, S. G. Kang, H. S. Moon, H. Park, I. T. Kim and S. G. Lee, *Appl. Surf. Sci.*, 2015, **351**, 193-202.
83. J. H. Lee, S. G. Kang, I. T. Kim, S. Kwon, I. Lee and S. G. Lee, *Theor. Chem. Acc.*, 2016, **135**, 1-9.
84. C. Di Valentin, L. Ferrighi and G. Fazio, *ChemSusChem*, 2016, **9**, 1061-1077.
85. L. Yang, S. Jiang, Y. Zhao, L. Zhu, S. Chen, X. Wang, Q. Wu, J. Ma, Y. Ma and Z. Hu, *Angew. Chem. Int. Ed.*, 2011, **50**, 7132-7135.
86. L. Wang, H. Dong, Z. Guo, L. Zhang, T. Hou and Y. Li, *J. Phys. Chem. C*, 2016, **120**, 17427-17434.
87. H. R. Jiang, T. S. Zhao, L. Shi, P. Tan and L. An, *J. Phys. Chem. C*, 2016, **120**, 6612-6618.
88. Z. W. Liu, F. Peng, H. J. Wang, H. Yu, W. X. Zheng and J. Yang, *Angew. Chem. Int. Ed.*, 2011, **50**, 3257-3261.
89. C. Zhang, N. Mahmood, H. Yin, F. Liu and Y. Hou, *Adv. Mater.*, 2013, **25**, 4932-4937.
90. I. Shimoyama, T. Hakoda, A. Shimada and Y. Baba, *Carbon*, 2015, **81**, 260-271.
91. X. Zhang, Z. Lu, Z. Fu, Y. Tang, D. Ma and Z. Yang, *J. Power Sources*, 2015, **276**,

222-229.

92. X. Bai, E. Zhao, K. Li, Y. Wang, M. Jiao, F. He, X. Sun, H. Sun and Z. Wu, *Carbon*, 2016,

105, 214-223.

93. N. Yang, X. Zheng, L. Li, J. Li and Z. Wei, *J. Phys. Chem. C*, 2017, **121**, 19321-19328.

94. Z. W. Liu, X. Fu, M. Li, F. Wang, Q. Wang, G. Kang and F. Peng, *J. Mater. Chem. A*, 2015, **3**, 3289-3293.

95. P. Zhang, X. Hou, J. Mi, Y.He, L. Lin, Q. Jiang and M. Dong, *Phys. Chem. Chem. Phys.*, 2014, **16**, 17479-17486.

96. L. Zhang, J. Niu, M. Li and Z. Xia, *J. Phys. Chem. C*, 2014, **118**, 3545-3553.

97. Z. Lu, S. Li, C. Liu, C. He, X. Yang, D. Ma, G. Xu and Z. Yang, *RSC Adv.*, 2017, **7**, 20398-20405.

98. Y. Li, C. He and L. Zhang, *Solid State Commun.*, 2017, **267**, 33-38.

99. J. Liang, Y. Jiao, M. Jaroniec and S. Z. Qiao, *Angew. Chem. Int. Ed.*, 2012, **51**, 11496-11500.

100. J. Song, T. Liu, S. Ali, B. Li and D. Su, *Chem. Phys. Lett.*, 2017, **677**, 65-69.

Chapter 3

Chapter 3 : Instruments & Apparatus

3.1 Experimental set up:

3.1.1 Oven

Ovens are commonly used for heating. Starting materials are stoichiometrically mixed and annealed in the furnace within the temperature range of 50 – 300 ^{0}C for 15 – 20 h. Thorough intermediate grinding is an important step for phase uniformity. The temperature controller usually controls the rate of heating and maintains the temperature with an accuracy of ±0.5 ^{0}C. **Fig.3.1** shows the digital image of the oven used. A low temperature oven was used for drying the samples and also for certain hydrothermal reactions.

Fig.3.1: Digital images of a Oven

3.1.2. Magnetic Stirrer

The magnetic stirrer can stir the magnetic bit within the solution of the beaker through a revolving magnetic arrangement attached with it. A heater arrangement associated with the stirrer can heat the solution at a desired temperature and the temperature is controlled by a knob as shown in **Fig.3.2**.

Fig.3.2: Digital image of a magnetic stirrer

3.2 Characterization tools:

3.2.1 X–Ray diffractometer (XRD):

In 1895, x-ray is discovered by Röentgen. From the year 1912, the application of x–ray has started when the wave nature of x–ray was recognized from the x–ray diffraction by any crystals. X–ray diffraction by the different set of planes has been applied to identify crystal structures. The structural characterization of synthesized samples is carried out by recording the X–Ray Diffraction pattern of the samples. XRD pattern was taken using Cu K_α radiation (λ = 1.5406˚A) (Rigaku–Ultima–III). The photograph is shown in the figure 3.3 below. The basic law involved in the crystal structure analysis is the Brag's law of diffraction. When monochromatic X–rays incident upon the atoms in a crystal lattice, each atom acts as a source of scattering. The crystal lattice acts as series of parallel reflecting planes and the reflected beams at certain angles form constructive interference which is an integral multiple of λ. This condition called Bragg's law is given by the relation,

(3.1)

Where *n* is the order of diffraction and *d* is the spacing between two consecutive planes *and* λ is the wavelength of the x–rays, and Θ is the glancing angle. XRD studies of any sample give a whole range of information about the crystal structure, average crystallite size and various stresses in the thin film. Generally, the obtained experimental data of the sample are compared with the standard inorganic crystal structure database (ICSD) to confirm the phase purity of our synthesized samples.

From the shift in peak position, one can calculate the change of d–spacing, which signify the change of lattice constant under inhomogeneous or homogeneous strain. Inhomogeneous strain differs from crystallite to crystallite or within a single crystallite.

This causes the peak broadening which increases with *sinθ*. This broadening also occurs from the crystalline size effect, but here the broadening is independent of *sinθ*. If there is no inhomogeneous strain, the crystallite size, D can be calculated from the Scherrer's formula:

$$\frac{\quad}{\quad} \qquad (3.2)$$

Where, β is the full width of height maximum (FWHM) of a diffraction peak, k is the Scherrer constant and θ is the diffraction angle [1–3].

Fig. 3.1 the X-ray diffractometer – Rigaku Ultima III.

.

3.2.3 X–ray photoelectron spectrometer (XPS)

Chemical Composition of the synthesized nanostructure, charge state of dopants, and purity of sample were analyzed by X–ray photoelectron spectroscopy (XPS, Specs, Germany). In photoelectron spectroscopy, photons are used to eject electrons from the bulk materials. Usually monochromatic, low energy X–rays are used to irradiate the sample which results in photoelectron emission from the atoms of the sample's surface and the kinetic energy distribution of the ejected photoelectrons is directly measured with the help of an electron spectrometer. As each surface atom possesses core–level electrons, the binding energy of each core–level electron is the characteristic of the atom and its specific orbit [1].

Since the energy of the incident X–rays is known, the measured kinetic energy of a core–level photoelectron peak can be directly assign to its characteristic binding energy. Therefore, XPS provides a means of elemental identification and the use of a standard set of sensitivity

factors also provides a surface atomic composition. The kinetic energy (E_k) of these electrons is measured and their binding energy (E_b) can be calculated.

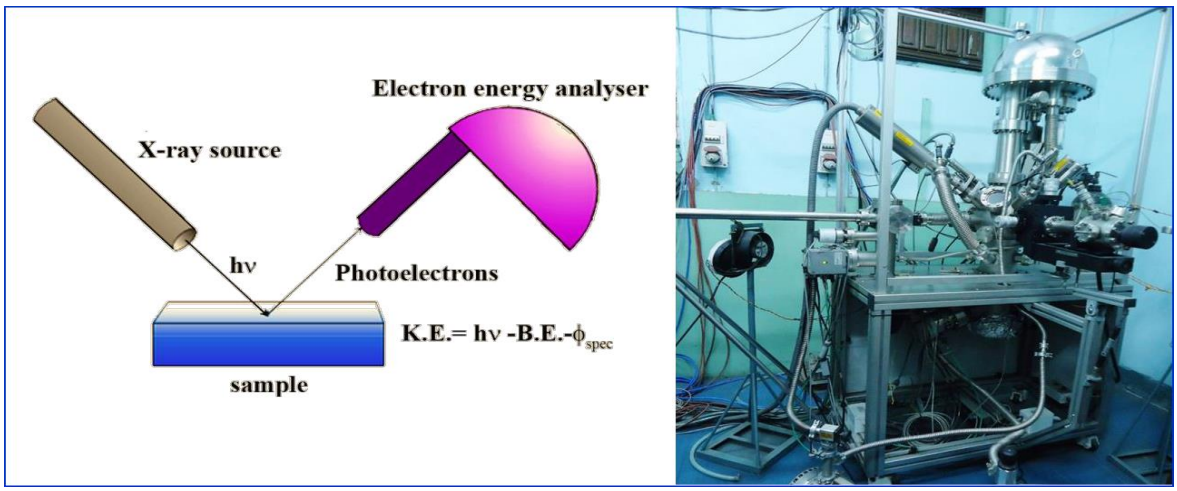

Fig. 3.4 Left: Schematic of the photo-excited electron emission in XPS instrument. Right: SPECS, HAS

3500 XPS instrument

The determination of the electron binding energy is the goal of the spectrometer which is found using the following relation:

(2.4)

Where, *hv* is the X-ray energy (known) and E_k is the kinetic energy of the photoelectrons (measured) [4]. The mechanism of electron emission is shown schematically in figure 3.6 (a).

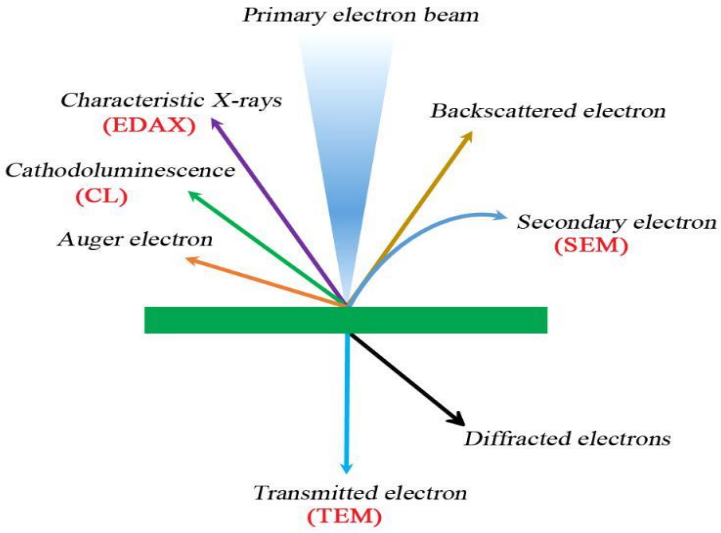

Fig. 3.5 Effects of electron bombardment on the material

Since binding energy of a photoelectron is profound to chemical surroundings of the atom, the chemical shifts in the binding energies of the photoelectron peaks arise due to the variations in electrostatic screening experienced by core level electrons. Various oxidation state, coordination number and molecular environment provide different chemical shifts that can be measured in a high-resolution (HR) XPS spectrum. In the present work, the chemical state of the constituent elements is examined by X–ray photoelectron spectroscopy using monochromatic Al K_α ($h\nu$ = 1486.6 eV) X–ray source and a hemispherical analyzer (SPECS, HSA 3500). The photograph is shown in figure 3.4 (b).

3.2.4 Field emission scanning electron microscope (FESEM):

In standard electron microscopes, electrons are mostly generated by heating a tungsten filament (electron gun). They are also produced from a crystal of LaB_6. The use of LaB_6 results in a higher electron density in the beam and a better resolution than that with the conventional used device. In a field emission (FE) electron microscope, no heating but a so–called "cold" source is used. Field emission microscope is a type of electron microscope that is usually employed to investigate the surface of a sample by scanning it with a high energy beam of electrons. Here, the wave properties of electrons ($\lambda = h/p$, λ associated with a beam of electrons of momentum p) are used to obtain resolution. If the electrons are accelerated through a potential difference V, they acquire energy.

When an electron beam interacts with the atoms of a nano structures sample, each incident electron undergoes two types of scattering elastic and inelastic. In elastic scattering, only the trajectory changes and the kinetic energy and velocity remain constant. In the case of inelastic scattering, the incident electrons displace electrons from the sample orbits around nuclei of atoms [1]. The electron interacts with the sample produces signal about the sample's morphology, composition and other properties. The morphologies of the synthesized nanomaterials are characterized with the help of field emission scanning electron microscopy (FESEM, S–4800).

So V = 100,000 V leads to $\lambda = 3.9 \times 10^{-12}$ m, which is about a hundredth of the separation of the atoms in molecules (~0.25 nm) or crystals [1].

In FESEM, the electron beam passes through objective lens deflect horizontally and vertically so that the beam scans the surface of the sample [Figure 3.6 (right)]. As the electrons penetrate the surface of the sample, a number of interactions occur that can result in the emission of electrons or photons from or through the surface. The generated secondary electrons are collected by the detector and converted into voltage. The amplified voltage is applied to the grid of the CRT which changes the intensity of the spot light. In this way an image is produced on the CRT; every point that the beam strikes on the sample is mapped directly onto a corresponding point on the screen [1, 6–7]. The schematic diagram of FESEM is presented in figure 3.6 (right). When an electron beam interacts with the atoms of a nano structures sample, each incident electron undergoes two types of scattering elastic and inelastic. In elastic scattering, only the trajectory changes and the kinetic energy and velocity remain constant. In the case of inelastic scattering, the incident electrons displace electrons from the sample orbits around nuclei of atoms [1]. The electron interacts with the sample produces signal about the sample's morphology, composition and other properties. The morphologies of the synthesized nanomaterials are characterized with the help of field emission scanning electron microscopy (FESEM, S–4800). The photograph of the instrument is shown in figure 3.6 (left).

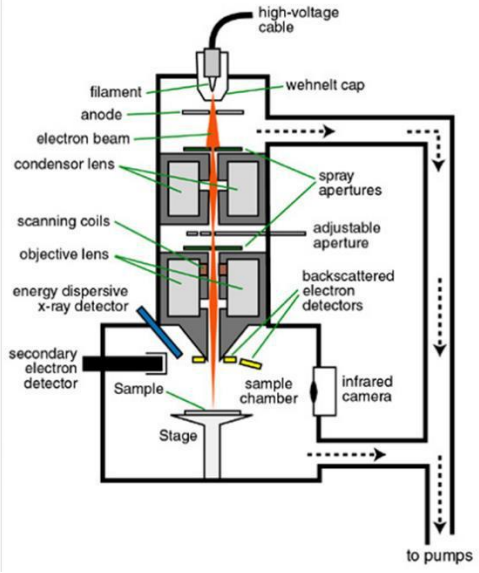

Figure 3.6 Left: Hitachi S4800 FESEM with EDX attachment

Right: Simple schematic of FESEM instrument

Energy Dispersive X–Ray (EDX) is one of the most versatile tools for analyzing the compositions of the synthesized samples. It is sometimes referred to also EDS or EDAX analysis. EDX is the integrated feature of both SEM and TEM. During EDX analysis, the specimen is bombarded with an electron beam inside electron microscope. The bombarding electrons collide with the specimen atom and knock some of them off in the process. The electrons vacated from the inner shell are eventually filled with the higher energy outer shell electrons and emit X–ray in this method. In this run, X–rays emitted from atoms represent the characteristics of the elements, and their intensity distribution represents the thickness–projected atom densities in the specimen. EDAX is a very important tool for identifying the chemical composition of a specimen [1, 6].

3.2.5 Transmission electron microscope (TEM):

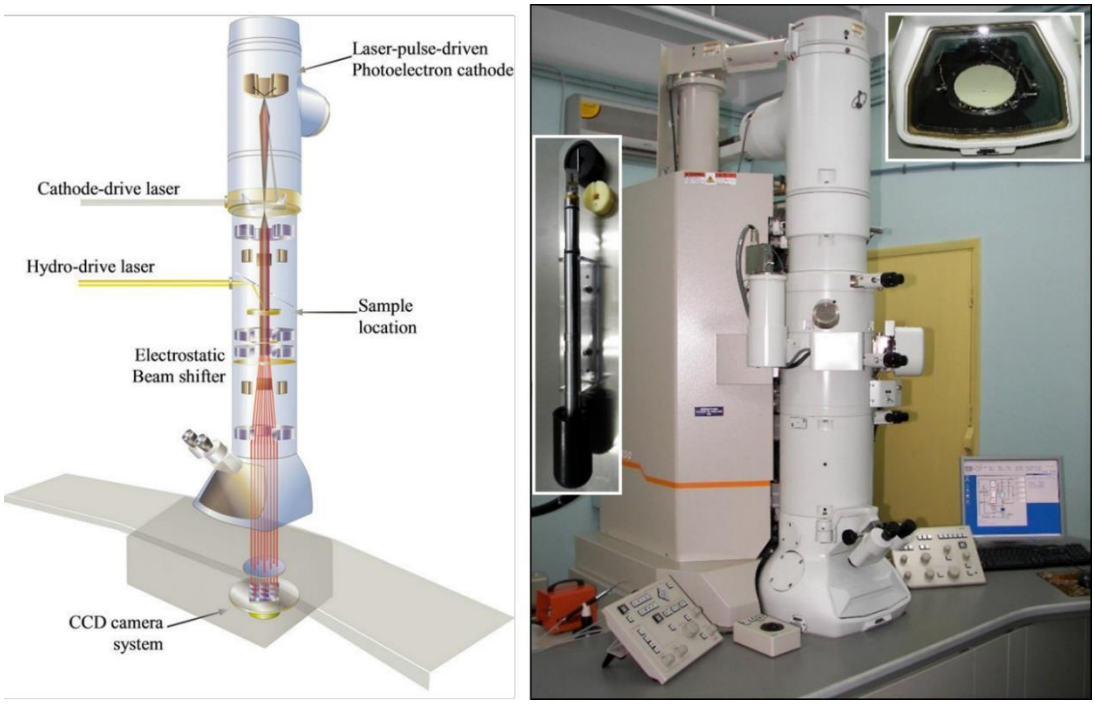

Figure 3.7 Left: Layout of optical components of basic TEM instrument.

Right: JEOL JEM-2100 HRTEM

Transmission electron microscope (TEM) is a unique tool in characterization of materials crystal structure and microstructure simultaneously by electron diffraction and imaging techniques. The basic TEM instrumentation is summarized in Figure 3.7 (left). The accelerating voltage is considerably higher than in an FESEM and is typically 100–300 kV. The benefits of high voltage improve imaging resolution and also penetration depth which facilitates the ability to study thicker samples. The specimen thickness must be no more than a few hundred nanometers and is usually in the Carbon coated copper grid of 3 mm diameter. The sample specimen is located between the pole pieces of the objective lens. The combination of the objective lens and the projector lens system provides an overall magnification of around 10^6. Along with that high resolution transmission electron

microscopy (HRTEM) is used to visualize the lattice images of the crystalline material which allow the direct characterization of the sample's atomic structures. The resolution of HRTEM is ~1 nm or less [1].

The contrast in high magnification image shows the periodic fringes. These fringes represent direct resolution of the Bragg diffraction plane that possesses interplanar spacing greater than the lateral spatial resolution. The selected area electron diffraction (SAED) of a small area of 0.1 μm diameter helps to determine the crystal structure of different parts of the sample. Basically diffraction patterns are distinguishable as sport pattern from single crystal diffraction zones or ring patterns are obtained from the randomly oriented crystal aggregates (polycrystalline). The *d* spacing of the planes corresponding to the rings can be determined by the following equation: $Dd = L\lambda$, where *D* is the ring diameter of the electron diffraction pattern, *L* is the effective camera length, λ is the de Broglie wavelength of the accelerating electrons and *d* is the interplanar spacing. The morphologies of the as synthesized nanomaterials were characterized with high resolution transmission electron microscopy (JEOL JEM-2100) [1, 7].

3.2.6 Raman spectrometer:

Vibrational properties of material as well as further information about phonon confinement, structure, phase, grain size etc. can be extracted using Raman spectroscopy. When a monochromatic radiation is scattered by molecules, a small fraction of the scattered radiation is detected to have a different frequency from the incident one due to the inelastic scattering. This down converted frequency shift is known as Strokes shifted scattering. Whereas Anti–strokes shift scattering results when the incident radiation absorbs a phonon and emerges with higher energy. In a Raman Spectroscopy, an intense monochromatic

radiation, i.e., a laser source is incident on the sample. The weak scattered light is passed through the monochromator to discard the Raleigh scattering and photo detectors detect the Raman shifted wavelength. The phonon confinement in a material can be found as the shift in the Raman line frequencies from the bulk material. Acoustic modes of bulk materials are not observable because of their low frequencies but in case of nanostructured material it appears in the measurable range. The frequency of the acoustic mode is inversely proportional to the size of the particles. Confinement of optical phonon results in the frequency shift and asymmetrical broadening of transverse and longitudinal optical mode line shape [1, 8].

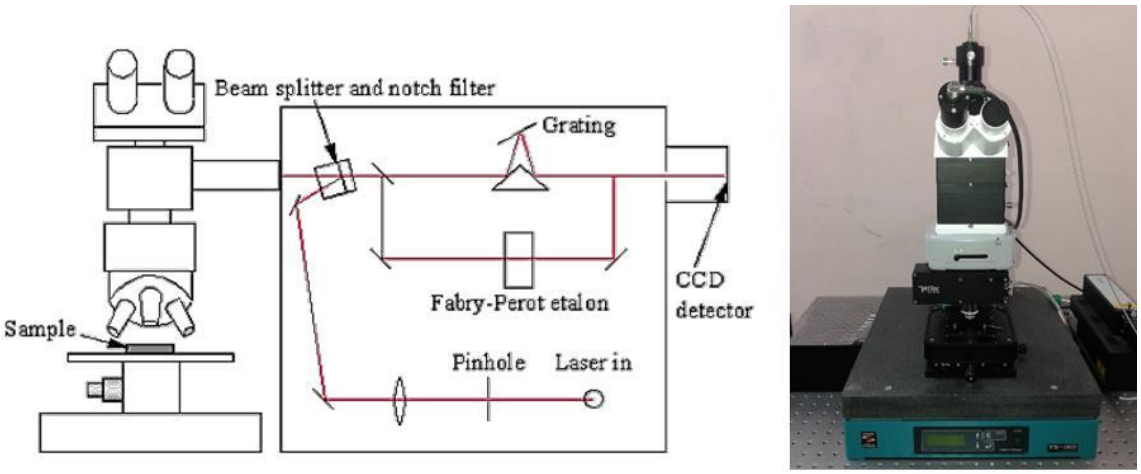

Figure 3.8 Left: Block diagram of the optical system of a spectrophotometer. Right: WITec alpha 300RS RAMAN spectrometer

Chapter: 4

rGO wrapped aCNT as a promising materials for ORR electrocatalyst

Abstract

In search of alternatives of Platinum-based electrocatalys, carbon - carbon based composites are under recent research focus. We, therefore, in this study, have addressed and explored the electrochemical performances of aCNT@rGOnanocomposites towards oxygen reduction reaction. The successful preparation of rGOwrapped aCNTs was testified by field emission scanning electronmicroscope (FESEM), transmission electronmicroscope (TEM), Raman spectroscopy and X-ray photoelectron spectroscopic (XPS). It is found that rGO wrapped aCNTs shows better catalytic activity that pristine aCNTs, which may be attributed to the surface functionalization and van-der-walls interaction between the components and higher conductivity of rGO in the composite.

4.1 Introduction

The electrochemical energy storage and conversion has played a vital role in solving theproblems arisen from the global energy demand and environmental impact of traditional fossil fuel. Among current energy storage technologies, fuel cells [including proton exchangemembrane fuel cells (PEMFCs), direct methanol fuel cells (DMFCs), direct formic acid fuelcells (DFAFCs) *etc.*]1 and metal-air (including Li-air, Mg-air, Al-air, Zn-air, and so on)batteries2 exhibit both high energy density and power density, which make them highlyattractive for energy storage and conversion applications.As the vital process in practical operation of fuel cells and metal-air batteries (thedischarge process), electrochemical oxygen

reduction reaction (ORR) has received extensive attentions for its highly complicated mechanism. ORR is the key limiting factor in the energyconversion efficiency of fuel cells, and also critical for better understanding of the reactionmechanism of oxygen electrode in metal-air batteries6. The sluggish kinetics of ORR makescatalysts highly demanding. By consuming the electrons from anode, the cathodic ORRalmost determines the discharge voltage of the whole battery. Traditionally, platinum (Pt)based noble metal catalysts that possess high activity and favorable stability were viewed asthe best ORR catalyst, receiving tremendous scientific interests during the early years.

However, it is well known that Pt-based catalysts suffer from drawbacks like scarcity, highcost, poor durability and easily inactivated by CO poisoning. Therefore, a lot of effortshave been devoted into the design and discovery of metal-free ORR catalysts as thealternatives of traditional Pt-based catalysts, which shows great influence on the developmentof fuel cells and metal-air batteries.Except for experimental investigations on the synthesis and applications of promisingmetal-free catalytic materials, theoretical simulations from first-principles calculation also play an important role in mechanistic explanation as well as design and prediction of novel metal-free ORR catalysts. The number of publications on ORR keeps increasing and remains great advantage over other electro-catalysis processes, such as oxygen evolution reaction (OER), hydrogen evolution reaction (HER) and carbon dioxide reduction reaction (CO_2RR). For fuel cells, ORR taken place in H_2O_2 fuel cells is of the most frequently studied.

Metal-free catalysts are materials totally composed of non-metal elements. Among them,carbon-based ORR catalysts are the most extensively investigated. There are great amount oftheoretical work in revealing the potential of B, N, Si, P and S single-doped or multi-dopedcarbon nanomaterials as ORR catalysts. Except the carbon-based nanomaterials, some binaryalloy

nanomaterials with stable crystalline structure (such as IIIA-VA and IVA-VIA2D-composites) have also shown great potential in electro-catalysis as reported in recentyears. Meanwhile, the defects, surface modification or hybridization induced ORR catalyticactivity in metal-free nanomaterials was also revealed by theoretical work.

4.2 Experimental details

4.2.1 Amorphous carbon nanotube preparation

The a-CNTS used for adsorption of Resorcinol and Arsenic were synthesised by a low temperature assisted process described in our previous work 20, where, certain amount of ammonium chloride and ferrocene, all analytically pure grades, were taken and thoroughly mixed in a mortar for 30 minutes. The mixture was then taken in a Borosil 250 mL glass beaker. A glass petridish was kept over the beaker as a cover to avoid immediate evaporation of ferrocene when the mixture was heated. The beaker was then inserted into an air furnace maintained at 250 °C. The heating was continued for 30 minutes and the sample was allowed to cool naturally. The resultant black powder was washed consecutively by diluted HCl and deionized water to remove the presence of trace amount of iron and filtered. The black residue was finally dried for 24 h at temperature 80 °C.

4.2.2 Reduced graphene oxide formation

Graphene oxide (GO) was synthesized from graphite powder using modified Hummer's method. In brief, 1 g of graphite and 0.5 g of sodium nitrate were mixed together followed by the addition of 23 ml of conc. sulphuric acid under constant stirring. After 1 h, 3 g of $KMnO_4$ was added gradually to the above solution while keeping the temperature less than 20°C to prevent

overheating and explosion. The mixture was stirred at 35 °C for 12 h and the resulting solution was diluted by adding 500 ml of water under vigorous stirring. To ensure the completion of reaction with $KMnO_4$, the suspension was further treated with 30% H_2O_2 solution (5 ml). The resulting mixture was washed with HCl and H_2O respectively, followed by filtration and drying, graphene oxide sheets were thus obtained. Then, In 40 ml DI water, we added 5mg of GO power then sonicate it for next 2 h. Then after 15 minutes of starring transfer it to the autoclave at 180 degree centigrade for 12 h then we will collect the sample, and will get purerGO after using vacuumfiltration.

4.2.3 aCNT@rGO composite preparation

In 40 ml DI water, we added 5 mg of GO power then sonicate itfor next 2 h. Hence we add 15 mg aCNT to the solution, then after 15 minutes of starring transfer it to the autoclave at 180 degree centigrade for 12 h then we will collect the sample, and will get pure rGO after using vacuum filtration.

4.3 Result and discussion

4.3.1. Characterization

4.3.1.1 FESEM study

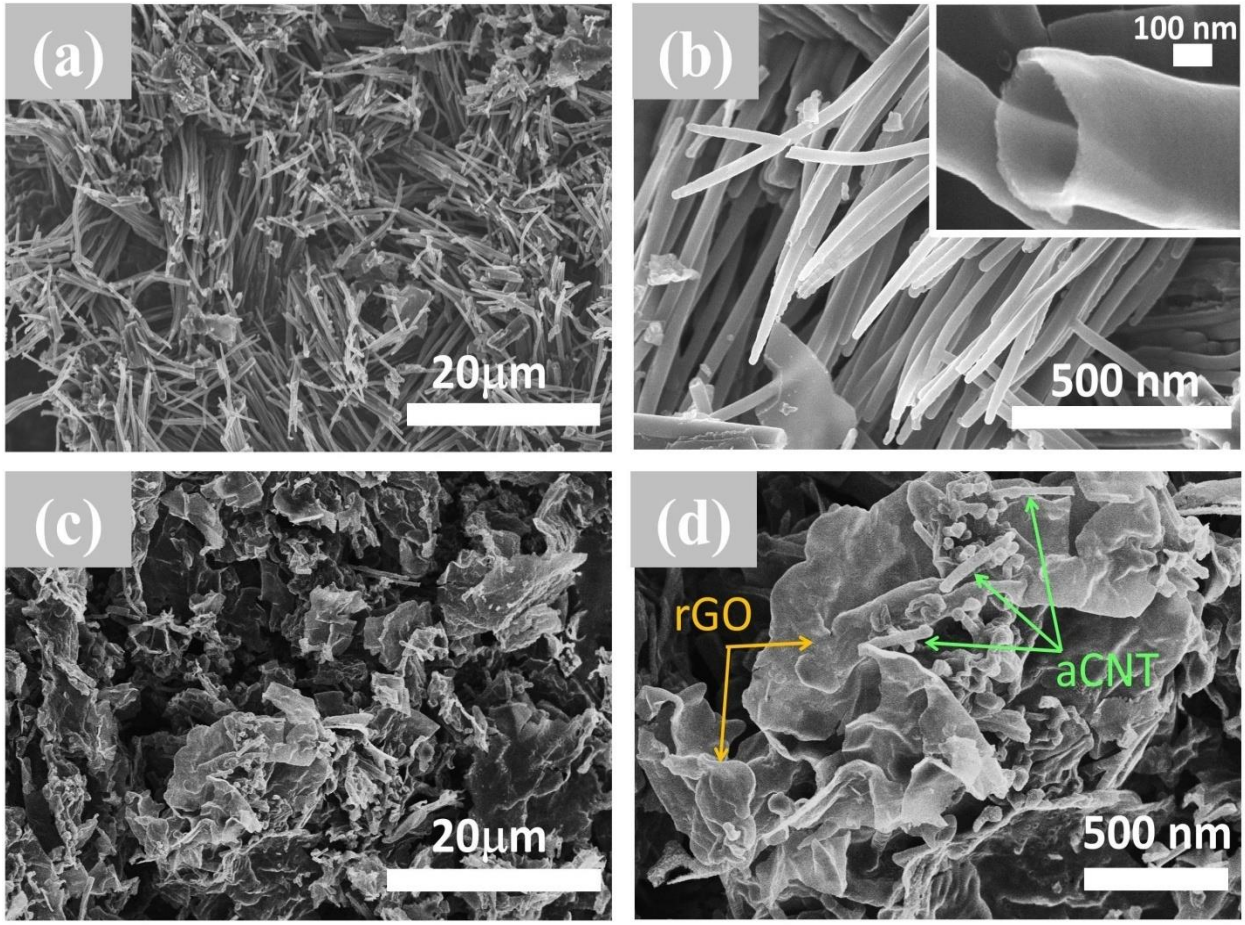

Figure 1. (a)Low and (b) high magnification FESEM images of aCNTs and (c) low and (d) high magnification FESEM iamges for aCNT@rGO nano composites.

Morphologies of the pristine aCNTs and the aCNT@rGOnanocomposite are characterized by FESEM as shown in Fig.1. It can be observed in Fig. 1b that the diameter of the CNTs is about 40 to 60 nm. The image corresponding to Fig.1(c) and 1(d) are showcasing the rGO layer sheet

blanket covering the bottom aCNTs in different low and high magnifications forming the hybrid composite carbon nanostructure. Due to the undulating morphology of the bunched asymmetrically distributed aCNTs, it generates a curvy surface morphology for the top assembled rGO layers which enhances the edge effect in rGO even more as evidenced from pronounced folding and wrinkling. The curling of the rGO edges with aCNTs leads to the enhancement of the ripple and adherence of the rGO sheets in the hybrid assembly. The protruding edge sites of the boundary peripheral region of rGO sheets over aCNTs can be observed clearly from the figures demarcated by the arrowheads.

4.3.1.2. Raman study

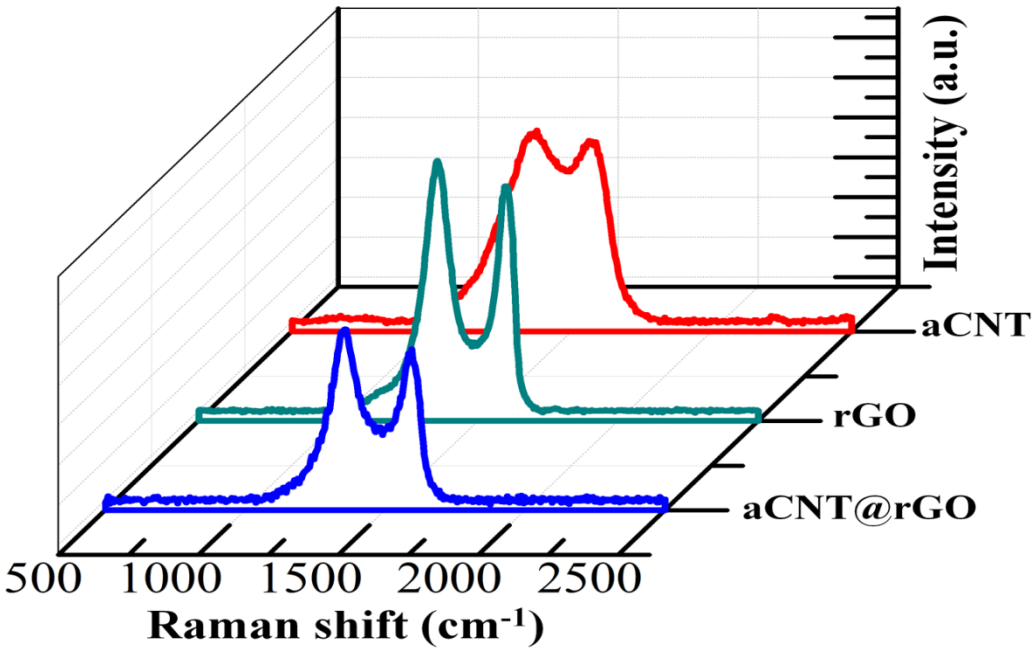

Figure 2. Raman spectrum of the aCNT@rGO nanocomposites along with pristine rGO and aCNTs samples

Fig. 2reports the Raman spectrum, for the aCNT, rGO and aCNT@rGO electrodes. Raman measurements, as shown in Fig.2, provide insight into the morphology of the resulting electrodeposited electrodes.The Raman spectrum of rGO exhibits characteristic D and G band peaks around 1358 and 1596 cm^{-1}, corresponding to the breathing mode of k-point phonons of A_{1g} and tangential stretching mode of the E_{2g} phonons of sp^2 atoms, respectively. Distinctive D and G bands are observed for other samples also. The intensity ratio of the D to G bands (I_D/I_G = disorder parameter) is found to be 1.02 and 1.09 respectively for aCNTs and rGO. It is interesting to observe that the (I_D/I_G) ratio is increased to 1.14 for the aCNT@rGOnanocomposites demonstrating the formation of large number of small sp^2 domain. The Raman spectrum of aCNT@rGOnanocomposite is shown in Fig. X4(b).

4.3.1.3. HRTEM study

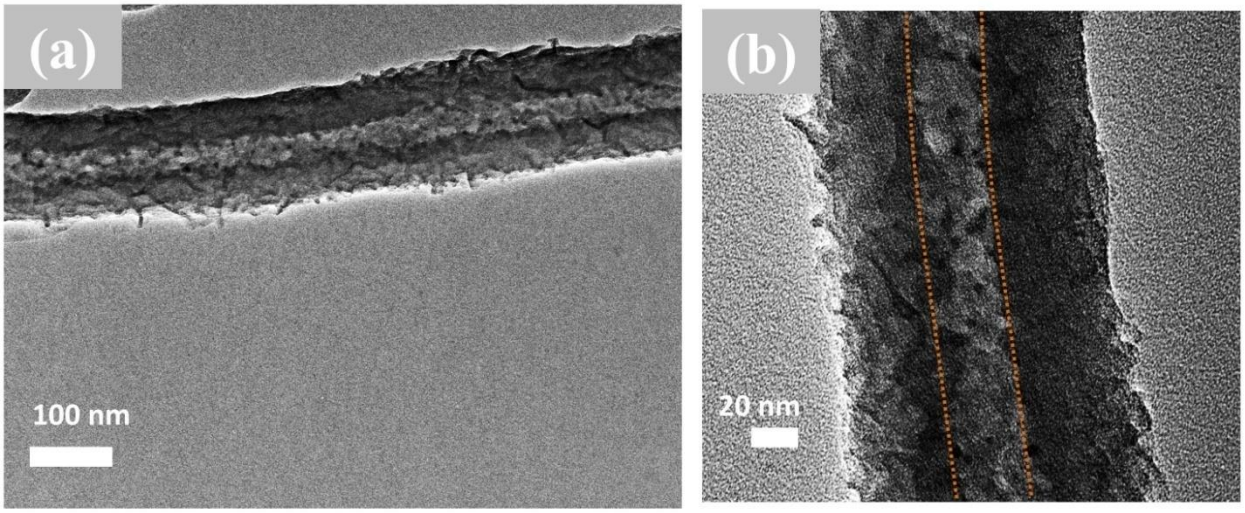

Figure 3.(a) The TEM image of the aCNT@rGO nanocomposite, (b) Magnified TEM images of a single aCNT coated with a rGO layers

TEM images of the aCNT@rGOnanocomposite are shown in Fig.3. As shown in Fig.3a, the aCNT core and the highly wrinkle rGO sheath resembling caterpillar-like morphology can be clearly seen. Fig.3b,c show the TEM images of a single aCNTs coated with wrinkle rGO at different magnifications. It can be seen that the rGO layer is composed of numerous tiny nanoflakes, which are interconnected and uniformly distributed on the surface of the aCNTs. The thickness of the rGO layer is estimated to be about 2-3 nm as shown in Fig.3b.

4.3.1.4. XPS Analysis

Quantitative information related to the chemical state, type, and extent of the surfaces of the aCNT@rGOnanocomposites are investigated by X-ray photoelectron spectroscopy (XPS), as shown in Fig. 4. Typically, the peaks at 284.6, 286.8 and 288.7eV are assigned to the C-C, C-O

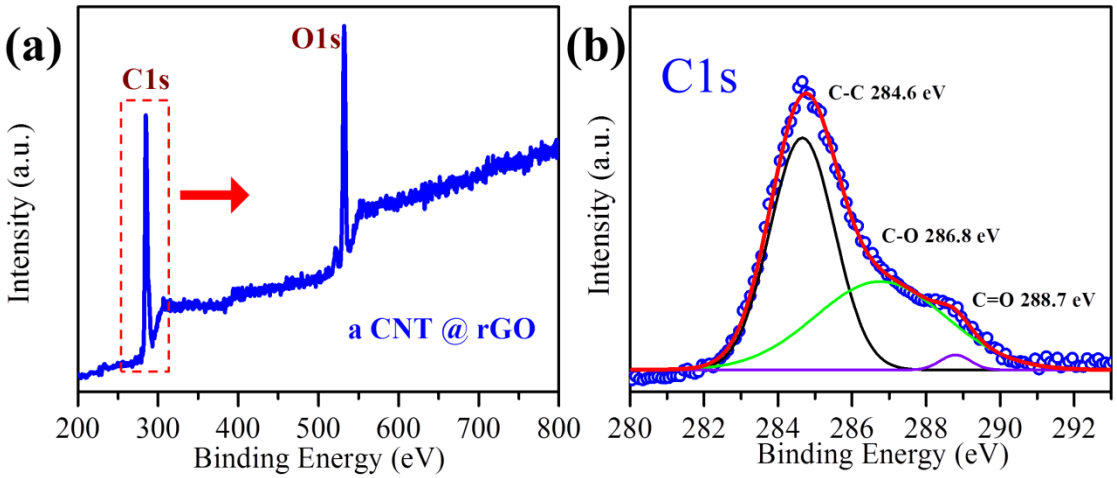

Figure 4.(a) X-ray photoemission spectroscopy (XPS) profiles of aCNT@rGO hybrid nanocomposite sample, (b) Curve fit of C1s peak of aCNT@rGO.

and C=O bonds, respectively. After thehydrothermal reduction process,the peakintensity ofthe C– O bond decreased in the composite system (Fig. 4b). Quantitative analysis of the XPS results

suggests that the proper growth of rGO on aCNTs is attributed to the direct redox reaction between the metal ions and the aCNT@rGOnanocomposite.

4.3.2. Application

4.3.2.1.aCNT@rGO composite electrocatalyst for ORR

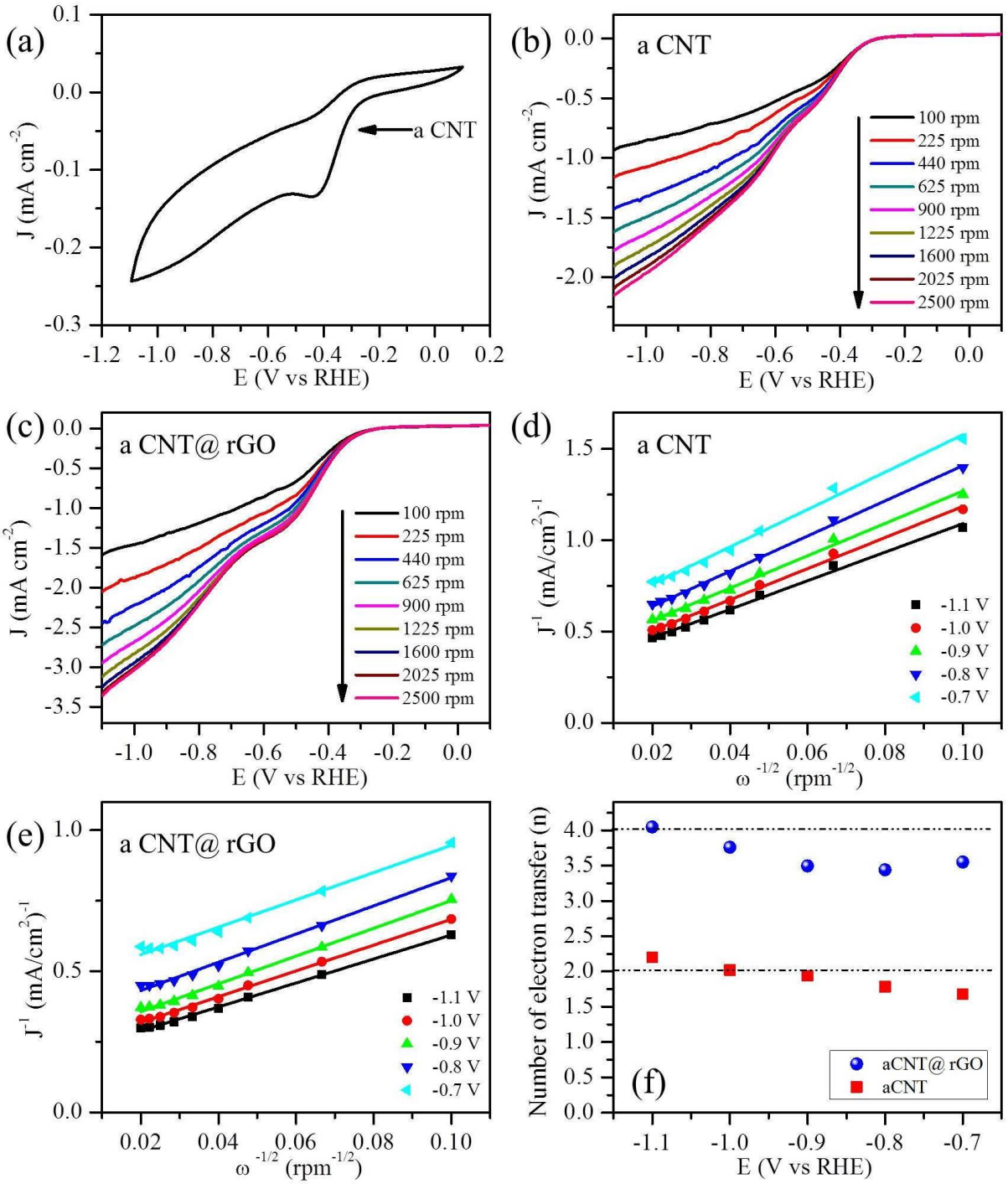

Figure.5 (a) CV for aCNT catalyst in O_2 saturated, (b-c) aCNT and aCNT@rGO composites in O_2 saturated 0.1 M KOH at a scan rate of 50 mV/s, LSV results of aCNT@rGO catalyst with different speed, (d-e) Koutecky–Lecivh plots of aCNT and aCNT@rGO catalyst and electron transfer number (n) vs. E(V vs. RHE).

We tested the ORR activities of the samples in the basic media (0.1 M KOH). ORR activities were measured by rotating disk electrode (RDE) and rotating ring-disk electrode (RRDE) technologies. For comparison, commercial platinum (20 wt%) on carbon black (Pt/C) (Johnson Matthey) was also tested in our early work.[30]. The catalytic activity of aCNTs towards ORR was also evaluated by CV (Fig. 5a) measurement. aCNT sample showed a well-defined reduction peak when the electrolytesolution is saturated with oxygen.

Fig. 5 shows the ORR results. According to the reported literature, the typical product exhibits the very high ORR activity and excellent durability in basic media. RDE voltammograms for the ORR on the typical product at the various rotation speeds (from 100 to 2500 rpm) was shown in the Fig. 5b. RDE voltammograms on the aCNT and aCNT@rGO at the various rotation speeds (from 100 to 2500 rpm) was shown in the Fig. 5b–c. From the Fig. 5b and 5c, the half-peak potential of the typical aCNTs and aCNT@rGOare only 90 and110 mV less than that of the Pt/C at the rotation speedof 2500 rpm, respectively.

According to the different rotation rates of RRDE testing, the Koutecky-Levich (K-L) theoryis applied to calculate the electron transfer number (n)[21, 22]. The diffusion-limited currentdensity (J_d) on RRDE was estimated by the K-L equation. Where J_k is the kinetic current density of the ORR; F is the Faradaic constant (96,485 C/mol); C_0 is the O_2-saturation concentration in the aqueous solution (1.2 x 10-6 mol/cm^3); D_0 is the O_2 diffusion coefficient in 0.1 mol/L KOH electrolyte (1.9 x 10^{-5} m^2/s); is the kinetic viscosity of the solution (0.01 cm^2/s) and is the electrode rotation rate (rpm). Fig. 5d-e shows the K–L plots at various potentials exhibit excellent linearity and parallelism, indicating consistent electron transfer and first-order reaction kinetics with regard to the concentration of dissolved oxygen.

$$\frac{1}{J_d} = \frac{1}{J_k} + \frac{1}{0.62} nFC_0 D_0^{2/3} \vartheta^{-1/6} \omega^{1/2} \quad (1)$$

The n value of aCNTs and aCNT@rGOcomposits for ORR were calculated to be ≈2.0 and 4.0, respectively, (K–L plot of $1/J_d$ vs.$1/\omega$ from -0.7 to -1.1 V vsRHE), suggesting the nearly two-electron transfer processes in case of aCNT system and nearly four-electron transfer processes for aCNT@rGO composite system accordance with the results of great ORR activity (Fig.5f).

4.4Conclusion

We developed a simple method for the synthesis of aCNT@rGO hybrid nanocomposites for catalysts on the basis of non-covalent interaction between rGO and CNTs. rGOnanosheets were uniformly distributed on the aCNTs with a wrinkle size distribution (2.0 – 4.0 nm) than on aCNTs (range from 40–60 nm in diameter with an average size of few μm). aCNT@rGOelectrocatalysts show higher electrochemical surface area (67.46 m2/g) and current density (425.0 mA mg−1) for methanol oxidation than pure aCNTs. aCNT@rGO catalysts exhibit better electrochemical activity and the catalyst has a higher electrochemical activity than commercial Pt/C catalyst for ORR in alkaline solution, and is almost the four-electron process in the ORR. All results demonstrate that aCNT@rGOare excellent catalysts for methanol electro-oxidation and oxygen reduction.

4.5 References

1. Z. Chen, D. Higgins, A. Yu, L. Zhang and J. Zhang, *Energy Environ. Sci.*, 2011, **4**, 3167-3192.

2. F. Cheng and J. Chen, *Chem. Soc. Rev.*, 2012, **41**, 2172-2192.

3. R. Padbury and X. Zhang, *J. Power Sources*, 2011, **196**, 4436-4444.

4. B. Wang, *J. Power Sources*, 2005, **152**, 1-15.

5. H. A. Gasteiger and N. M. Markovic, *Science*, 2009, **324**, 48-49.

6. M. Armand and J. M. Tarascon, *Nature*, 2008, **451**, 652-657.

7. Y. Wang and P. B. Balbuena, *J. Phys. Chem. B*, 2005, **109**, 14896-14907.

8. Y. Sha, T. H. Yu, Y. Liu, B. V. Merinov and W. A. G. III, *J. Phys. Chem. Lett.*, 2010, **1**, 856-861.

9. G. Wei, Y. Fang and Z. Liu, *J. Phys. Chem. C*, 2012, **116**, 12696-12705.

10. N. M. MarkovicÂ, T. J. Schmidt, V. StamenkovicÂ and P. N. Ross, *Fuel Cells*, 2001, 105-116.

11. J. A. Keith and T. Jacob, *Angew. Chem. Int. Ed.*, 2010, **49**, 9521-9525. 12. J. A. Keith, G. Jerkiewicz and T. Jacob, *ChemPhysChem*, 2010, **11**, 2779-2794.

13. V. Tripkovic, E. Skulason, S. Siahrostami, J. K. Norskov and J. Rossmeisl, *Electrochim. Acta.*, 2010, **55**, 7975-7981.

14. S. Suzuki, T. Onodera, J. Kawaji, T. Mizukami and K. Yamaga, *Appl. Catal. A-Gen.* , 2012, **427**, 92-97.

15. Z. W. Liu, F. Peng, H. J. Wang, H. Yu, C. L. Chen and Q. Q. Shi, *Catal. Commun.*, 2012, **29**, 11-14.

16. M. J. Janik, C. D. Taylor and M. Neurock, *J. Electrochem. Soc.*, 2009, **156**, B126-B135.

17. M. Winter and R. J. Brodd, *Chem. Rev.*, 2004, **104**, 4245-4269.

18. C. Sealy, *Mater. Today*, 2008, **11**, 65-68.

19. K. Gong, F. Du, Z. Xia, M. Durstock and L. Dai, *Science*, 2009, **323**, 760-764.

20. L. Dai, Y. Xue, L. Qu, H. J. Choi and J. B. Baek, *Chem. Rev.*, 2015, **115**, 4823-4892.

21. Z. Yang, Z. Yao, G. Li, G. Fang, H. Nie, Z. Liu, X. Zhou, X. Chen and S. Huang, *ACS Nano*, 2012, **6**, 205-211.

22. S. Zhao, J. Liu, C. Li, W. Ji, M. Yang, H. Huang, Y. Liu and Z. Kang, *ACS Appl. Mater. Inter.*, 2014, **6**, 22297-22304.

23. K. Zhou, W. Zhou, X. Liu, Y. Wang, J. Wan and S. Chen, *ACS Appl. Mater. Inter.*, 2014, **6**, 14911-14918.

24. X. Wang, J. Wang, D. Wang, S. Dou, Z. Ma, J. Wu, L. Tao, A. Shen, C. Ouyang, Q. Liu and S. Wang, *Chem. Commun.*, 2014, **50**, 4839-4842.

25. Z. L. Ma, S. Dou, A. L. Shen, L. Tao, L. M. Dai and S. Y. Wang, *Angew. Chem. Int. Ed.*, 2015, **54**, 1888-1892.

26. S. Chen, J. Y. Bi, Y. Zhao, L. J. Yang, C. Zhang, Y. W. Ma, Q. Wu, X. Z. Wang and Z. Hu, *Adv. Mater.*, 2012, **24**, 5593-5597.

27. H. L. Jiang, Y. H. Zhu, Q. Feng, Y. H. Su, X. L. Yang and C. Z. Li, *Chem. Eur. J.*, 2014, **20**, 3106-3112.

28. G. Girishkumar, B. McCloskey, A. C. Luntz, S. Swanson and W. Wilcke, *J. Phys. Chem. Lett.*, 2010, **1**, 2193-2203.

29. Y. Shao, S. Park, J. Xiao, J. Zhang, Y. Wang and J. Liu, *ACS Catal.*, 2012, **2**, 844-857.

30. M. M. Montemore, M. A. van Spronsen, R. J. Madix and C. M. Friend, *Chem. Rev.*, 2018, **118**, 2816-2862.

31. K. M. Ervin, I. Anusiewicz, P. Skurski, J. Simons and W. C. Lineberger, *J. Phys. Chem. A*, 2003, **107**, 8521-8529.

32. B. Ruscic, R. E. Pinzon, M. L. Morton, N. K. Srinivasan, M.-C. Su, J. W. Sutherland and J. V. Michae, *J. Phys. Chem. A*, 2006, **110**, 6592-6601.

33. B. B. Blizanac, P. N. Ross and N. M. Markovic, *Electrochim. Acta.*, 2007, **52**, 2264-2271.

34. K. Kato, T. Uda and K. Terakura, *Phys. Rev. Lett.*, 1998, **80**, 2000-2003.

35. A. Ziletti, A. Carvalho, D. K. Campbell, D. F. Coker and A. H. Castro Neto, *Phys. Rev. Lett.*, 2015, **114**, 046801.

36. J. S. Spendelow and A. Wieckowski, *Phys. Chem. Chem. Phys.*, 2007, **9**, 2654-2675.

37. X. Ge, A. Sumboja, D. Wuu, T. An, B. Li, F. W. T. Goh, T. S. A. Hor, Y. Zong and Z. Liu, *ACS Catal.*, 2015, **5**, 4643-4667.

38. P. Quaino, N. B. Luque, R. Nazmutdinov, E. Santos and W. Schmickler, *Angew. Chem. Int. Ed.*, 2012, **51**, 12997-13000.

39. R. Nagappan and M. Sanjeev, *J. Phys. Chem. C*, 2011, **115**, 18015-18026.

40. R. Nagappan and M. Sanjeev,*Advances in Physical Chemistry*, 2012, **2012**, 1-17.

41. A. Ignaczakd, R. Nazmutdinovc, A. Goduljana, L. M. de C. Pintoa, F. Juareza, P. Quainoe, E. Santosa and W. Schmicklera, *Nano Energy*, 2016, **29**, 362-368.

42. H. Shi, Y. Shen, F. He, Y. Li, A. Liu, S. Liu and Y. Zhang, *J. Mater. Chem. A*, 2014, **2**, 15704-15716.

43. K. M. Abraham and Z. Jiang, *J. Electroanal. Chem.*, 1996, **143**, 1-5.

Chapter 5

Chapter 5

5.1 Grand conclusion:

Electrocatalysis is a mild approach in energy conversion, which is recongnized as a effictive method to address the energy crsis and environment pollution. With the rapid development of computational methods and computing ability, combining experimental researches with theoretical simulations could effectively reduce the research period and cost, thus accelerates the commericalization of novel materials comparing with pure experimental trial-and-error. This strategy has already been successfully applied into design and discovery of catalysts for various electro-chemical reactions, such as nitrogen reduction reaction (N_2RR), CO_2RR, HER/HOR and ORR/OER. Among them, ORR catalysts have received the most attention due to it vital role played in cathode of fuel cells and Li-O_2 batteries. In this review, we have summarized the possible reaction mechanisms during ORR catalysts, and the novel metal-free catalysts proposed by computational investigations during the recent years. By exploring the origin of catalytic activity, we also summarized the design principles for metal-free ORR catalysts from the view of theoretical calculations. The theoretical simulation based on the first-principles calculations (density functional theory) can not only work as a supplement of experimental studies, but also have the potential as an independent part in designing and predicting novel metal-free materials for ORR.

5.2 Future scope:

For the further development ofmetal-free ORR catalysts through theoretical simulations and experimental characterization,there are still several points to be addressed as supplements for the current methods.

I. The corporation of explicit solvation model should be contained in a uniform simulation model. From the microscopic view, electrocatalysis is usually realized through heterogenerous reaction, involving the interface effect between liquid electrotyles, reactants and solid electrode. Due to the fact that the free energy landscape with the entropy effect is reasonable to describe a complete electrocatalytic reaction, thus it is necessary to construct a uniform simulation model that contains complete therodynamic and dynamic processes at the landscape of free energy. In fuel cells, water molecules (as H_3O+ in acid media or as reactant in alkaline media) plays a vital role in the reaction process. Hydrogen bond interaction has unnegligible influence on the adsorption of ORR intermediates although implicit salvation model can be taken into consideration. By making a clear comparsion of CO_2RR under vacuum, implicit solvation model and explicit solvation model, Cheng et al. demonstared that the potential map of intermediates under vacuum and implicit model is inaccuracy, especially if the -OH contained species existed.137 Explicit model revealed that the weak hydrogen bond between water and the adsorbed OH can stabilize the *OH-contained species adsorption. And the G(*OH) is usually taken as a scaling parameter to evluate ORR performance, which obvioulsy introduced ceterain computational errors. For nonaqueous Li-O_2 batteries, there is no hydrogen bonds involved, however, the function of electrolyte may also bring a ceterin effect on the adsorption of intermediates. Thus the energy correction of electrolyte molecules in free energy should be a necessary improvement for Li-O_2 batteries calculations.

II. The multi-scale simulation is a new trend for simulating the ORR process as well as designing new metal-free ORR catalysts. Atomic acitity site and transient reaction intermeidates are difficult to be directly observed and correlated with the experimental data. Thus multiscale simulation from microscopic activity site, reaction process to macroscopic current-voltage can provide a complete understanding on the ORR processes systemically. According to the basic parameters calculated from first-principles calculations, Vazquez-Arenas et al.138 and lkeshji et al.139 separately designed the multi-scale model to fully simulate the ORR process. Polarization curves, cyclic voltammetry (CV) and linear sweep voltammetry profiles can be simulated and

compared with the experimental results. Their results disclosed that not only the adsorption energy of intermediates, but also the activation Journal of Materials Chemistry energy should be considered to tune ORR performance above the valcano-top. No doubt themulti-scale simulations will provide more specific and more accurate descriptors that help toscreen excellent metal-free catalysts.

III. There still needs a reliable reference system due to the non-uniform status of ORR simulations in Li-O_2 batteries. Unlike the extensively studied ORR catalysis in fuel cells, ORR in Li-O_2 batteries is relatively less elusidated. Due to the many controversies and uncertainties in catalytic process, products as well as energetics, different methods will generate results that are highly different. As listed in for some of the most referred systems such as graphene and graphitic N doped grahene, different publications give ORR values that heavily vary from each other. Despite the errors comes from size of adsorbent and computational software, most of the differences come from the different treatment of energetic terms (like entropy and ZPE), the energy of Li atom, and the confirmation of final Li oxides. The lack of experimental measurement on discharge potential also accounts for the discrepancies. Thus, a versatile reference system and a uniform calculation standard for free energy terms are highly desired for the further development of theoretical simulation on metal-free cathode catalysts for Li-O_2 batteries. Meanwhile, another problem arisen from the summary of is that most of the reported metal-free catalysts exhibit high ORR overpotentials that limits the practical discharge voltages of the Li-O_2 batteries. Thus there is still great space for the development of novel metal-free cathode catalysts with outstanding discharge performance.

IV: For experimental sciences, it should be pointed out that our current quantum simulation models are still limited by the computing capability, which is confined into hundreds of atoms. On one hand, we should expand our simulation configurations to fit practical configurations. On the other hand, is it possible for experimenters to decrease the catalysts into atomic scale with precise synthesis of active sites? Meanwhile, synthesizing specific catalysts based on the theoretical materials design might be another challenge. Pursuit of catalytic efficiency and performance may be the ultimate goal in the experiments. Nevertheless, uncovering the mechanism behind ORR still need more detailed atomic characterization